Geophys. J. Int. (2002) **151,** 755–770

Controlled source apparent resistivity tensors and their relationship to the magnetotelluric impedance tensor

T. Grant Caldwell,[1,2] Hugh M. Bibby[1] and Colin Brown[2]

[1] *Institute of Geological and Nuclear Sciences, Gracefield Research Centre,* PO Box 30368, *Lower Hutt, New Zealand. E-mail: g.caldwell@gns.cri.nz*
[2] *Applied Geophysics Unit, National University of Ireland, Galway, Ireland*

Accepted 2002 June 19. Received 2002 May 15; in original form 2001 November 7

SUMMARY

The time-domain surface electric fields produced by a step current in collocated grounded sources can be represented by an apparent resistivity tensor defined by the relationship between the measured (time-varying) electric field and a reference field equal to the steady-state current density in a uniform half-space. A magnetic field response tensor is similarly defined for the horizontal components of the magnetic field. The 'magnetic field apparent resistivity tensor' is derived from a linear combination of the contractions of the outer product of the magnetic field response tensor. Frequency-domain apparent resistivity tensors are derived from the Laplace transforms of the corresponding time-domain electric and magnetic field response tensors. Both the frequency and time-domain tensors are independent of the source orientation where the sources can be approximated as (infinitesimal) dipoles. A simple combination of the frequency-domain (impulse response) tensors can be used to derive the controlled source magnetotelluric (CSMT) impedance tensor.

The magnetic field apparent resistivity tensor is a useful representation of the conductivity structure only where the source–receiver offset is much less than the diffusion or skin depth and behaves in a similar way to the 'early-time' apparent resistivity traditionally used to represent time-domain electromagnetic data. Numerical modelling results demonstrate that the (horizontal) magnetic field apparent resistivity is insensitive to the localized 3-D conductivity structures that are typically the target of exploration surveys. In contrast, the electric field apparent resistivity tensor depends sensitively upon the conductivity structure and is well behaved over the entire time or frequency range used in long-offset transient electromagnetic or CSMT measurements. By using the electric field apparent resistivity tensor, 'source effects' that hinder a conventional impedance tensor analysis of CSMT data can be avoided. Images of simple 3-D structures created from the invariants of the electric field apparent resistivity tensor (in either the time or frequency domain) provide a useful representation of the subsurface conductivity structure despite the simplicity of this imaging procedure. These images are independent of the coordinate system used to express the data and are, to a good approximation, independent of the current source orientations.

Key words: controlled source magnetotellurics, electrical resistivity, electromagnetic methods.

INTRODUCTION

Historically, the first step towards determining the conductivity structure in electromagnetic (EM) exploration surveys has been to transform measurements of the surface electric or magnetic fields into an apparent resistivity. Ideally, the apparent resistivity will provide a qualitative picture of the subsurface resistivity distribution that can be interpreted with a fair degree of confidence. It may also be regarded as a primitive, first attempt at inversion, which can be used as the starting point for a more sophisticated inversion. A good example of the use of apparent resistivity is provided by DC resistivity measurements. In the DC case, the apparent resistivity is defined by extending the laboratory definition of the resistivity of a homogenous material to situations where the applied current density is non-uniform (Keller & Frischknecht 1966; Bibby 1977; Zohdy 1978). In essence, the apparent resistivity involves a normalization procedure, which, for DC resistivity and active source EM methods, attempts to compensate for the effects of source–receiver geometry and source strength (Spies & Eggers 1986).

For frequency or time-domain EM (TDEM) techniques, the fields measured at the surface of a uniform half-space are non-linear functions of time (or frequency) and resistivity. Different choices of normalization for these techniques are possible. The approach usually taken in TDEM methods is to define the apparent resistivity from

the asymptotic early- and late-time behaviour of the homogenous half-space response for a particular component of the EM field (e.g. Spies & Frischknecht 1991). However, definitions of apparent resistivity that are based on the behaviour of a single EM field component perform poorly in 3-D situations as they depend on the polarization of the EM field.

The dependence of the apparent resistivity on polarization also occurs in DC resistivity surveys. This led Bibby (1977, 1986) to introduce the concept of an 'apparent resistivity tensor' to represent the electric field data produced in 'multiple-source bipole–dipole' surveys (e.g. Bibby *et al.* 1984; Risk *et al.* 1993). The DC apparent resistivity tensor provides a compact representation for the data produced by collocated grounded sources and a simple way of visualizing the surface electric field in 3-D situations (Bibby & Hohmann 1993). At large source–receiver offsets, where the current sources (grounded bipoles) can be approximated as (infinitesimal) dipoles, the apparent resistivity tensor is independent of source orientation (Bibby 1994; Li & Pedersen 1994). By using coordinate-invariant apparent resistivities derived from the tensor components, data analysis and interpretation can be conducted in a way that is independent of source orientation and the coordinate system used to express the data.

The same approach can be applied in the time domain where the electric fields produced by collocated grounded sources with different orientations can be represented by a time-varying or 'instantaneous apparent resistivity tensor' (Caldwell & Bibby 1998). In contrast to the early- and late-time apparent resistivities that have been used to represent TDEM or long-offset transient EM (LOTEM) data (e.g. Spies & Frischknecht 1991; Strack 1992; Hördt *et al.* 1992), the instantaneous apparent resistivity tensor is a well-behaved function of time. The instantaneous apparent resistivity differs from the early- and late-time representations in two essential ways. First, the instantaneous apparent resistivity is defined in terms of the total electric field vector rather than the transient part of the signal and, secondly, the analysis *requires* data from sources with different orientations.

By analysing the total electric field vector in a TDEM survey we are able to reintroduce the mathematical device used in DC resistivity methods of normalizing the measured electric field data with respect to the DC (or steady-state) current density in a uniform half-space. In the 'late-time' limit the instantaneous apparent resistivity tensor is equal to the DC apparent resistivity tensor. Time-dependent coordinate-invariant apparent resistivities derived from the tensor have a number of useful properties and can be used to create (distance–time) images of simple 3-D structures that show the main features of the subsurface resistivity structure despite the simplicity of this procedure (Caldwell & Bibby 1998).

In this paper, we will extend this method of analysis to the horizontal components of the magnetic field and show how a magnetic field apparent resistivity tensor can be derived from what we will call the 'magnetic field response tensor'. By introducing corresponding frequency-domain tensors, we are then able to analyse the relationship between the grounded source tensors and the magnetotelluric impedance tensor.

TIME DOMAIN TENSORS

The instantaneous apparent resistivity tensor

A detailed discussion of the instantaneous apparent resistivity tensor is given in Caldwell & Bibby (1998). We will briefly outline the key results from this paper below.

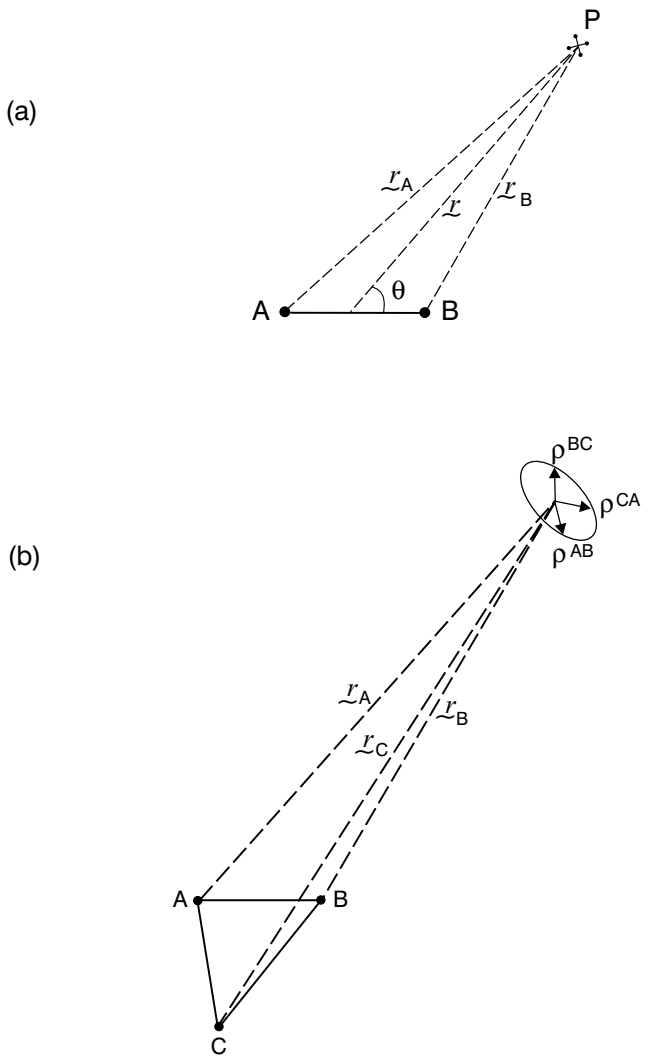

Figure 1. (a) Source and receiver configuration used in 'scalar' CSMT and LOTEM surveys where AB is the grounded source bipole. The electric field is measured at the point P using a pair of short orthogonal dipoles (typically 50–100 m long) as illustrated. The components of the magnetic field are normally measured using sensitive induction coils. (b) Source–receiver configuration for a multiple-source DC resistivity or 'tensor' LOTEM survey where three grounded bipoles (AB, BC and CA) arranged in a triangle are used as current sources. The instantaneous apparent resistivity tensor, represented by the ellipse, is determined from measurements of the electric field vectors arising from each source, the geometry of the array, and the magnitude of the current flowing in each source. The 'total field apparent resistivities' (ρ^{AB}, ρ^{BC} and ρ^{CA}) given by the ratio of $|\mathbf{E}|/|\mathbf{J}|$ (Zohdy 1978) arising from each source are plotted (schematically) as vectors in the direction of the measured electric field produced by the corresponding source bipole.

Where the resistivity distribution is 3-D, more than one EM field polarization is required to completely characterize the response. This can be achieved by using collocated grounded sources with different orientations as illustrated in Fig. 1. The time-varying electric fields produced by such an arrangement can then be compactly represented by a time-dependent apparent resistivity tensor defined by the relationship

$$\mathbf{E}(t) = \boldsymbol{\rho}_a(t)\mathbf{J} \tag{1}$$

between the electric field $\mathbf{E}(t)$ measured at a time t and the DC current density $\mathbf{J}$ in a uniform half-space corresponding to each current

source. The vector field **J** provides a time-independent method of normalizing the measured electric fields for the effect of source strength and geometry. For the situation shown in Fig. 1, the DC current density or 'source field' caused by the grounded bipole AB is given by

$$\mathbf{J}^{\mathrm{AB}} = I\left(\boldsymbol{r}_{\mathrm{A}}/r_{\mathrm{A}}^3 - \boldsymbol{r}_{\mathrm{B}}/r_{\mathrm{B}}^3\right)/2\pi. \tag{2}$$

If the source–receiver offset is much greater than the bipole length ($r = |\boldsymbol{r}| \gg |\boldsymbol{r}_{\mathrm{A}} - \boldsymbol{r}_{\mathrm{B}}|$) the source can be approximated by an infinitesimal dipole, which is characterized by its dipole moment I **ds**, where I is the current and the dipole is oriented in the direction of the vector **ds**. Note that **J** contains an implicit time dependence since the current is turned on at $t = 0$. This dependence can be made explicit by writing

$$\mathbf{J}(t) = U(t)\mathbf{J}, \tag{3}$$

where $U(t)$ is the unit (or Heaviside) step function.

Two different source orientations are required to determine the components of the apparent resistivity tensor. In the 3-D case, the tensor is non-symmetric and has three coordinate invariants. These invariants, along with a fourth parameter that depends on the coordinate system, express the information contained in this second-rank 2-D tensor. At any given instant the tensor can be represented graphically as an ellipse. This ellipse shows the locus of the tip of the electric field vector as a unit magnitude DC current density rotates through 360°. Thus, at each observation point and at each time instant we can represent our measurements by the 'apparent resistivity ellipse' as illustrated in Fig. 1. The properties of the apparent resistivity tensor ellipses are discussed in detail in Bibby (1986).

The lengths of the major ($\rho_{\max}$) and minor ($\rho_{\min}$) axes of the apparent resistivity ellipse correspond to two of the three coordinate invariants and define the 'principal' axes and values of the tensor. The third invariant corresponds to the angle between the current density **J** and the electric field when the electric field lies in the direction of the principal axes. The orientation of the ellipse major axis corresponds to the single coordinate-dependent parameter needed to complete the definition of the tensor. Functions of the invariants are also coordinate invariant. In particular, the coordinate-invariant apparent resistivity

$$P_2(t) = \{[\rho_{\max}(t)\rho_{\min}(t)]\}^{1/2} = \{\det[\boldsymbol{\rho}_{\mathrm{a}}(t)]\}^{1/2} \tag{4}$$

is the radius of the circle that has the same area as the ellipse. This parameter has a number of useful properties that gives it a special role in the analysis.

In a uniform half-space of resistivity ρ, the instantaneous apparent resistivity tensor is symmetric and is most naturally represented in a polar coordinate system centred on the sources. In this system of coordinates the tensor takes the simple form

$$\boldsymbol{\rho}_{\mathrm{a}}(t) = \begin{bmatrix} \rho_{rr} & \rho_{r\theta} \\ \rho_{\theta r} & \rho_{\theta\theta} \end{bmatrix} = \rho \begin{bmatrix} 1 - f(r/\delta)/2 & 0 \\ 0 & 1 + f(r/\delta) \end{bmatrix}, \tag{5}$$

where the subscripts denote the radial (r) and tangential (θ) components, r is the source–receiver separation and $f(r/\delta)$ is a function that expresses the time dependence of the electric field (Caldwell & Bibby 1998). For a step current switched on at $t = 0$ the function $f(r/\delta)$ is given by

$$f(r/\delta) = \mathrm{erf}(r/\delta) - (4/\pi)^{1/2}(r/\delta)\exp[-(r/\delta)^2], \tag{6}$$

where δ has the dimensions of distance and is given by

$$\delta = (4\rho t/\mu_0)^{1/2}, \tag{7}$$

t is the time (or 'delay') after the current is switched on and μ_{o} is the free space magnetic permeability (e.g. Spies & Frischknecht 1991).

The time behaviour of the coordinate-invariant apparent resistivities in a half-space is shown in Fig. 2. Note that the value of $P_2(t)$ remains almost constant over the entire time interval, the maximum difference between the half-space resistivity and $P_2(t)$ being ~6 per cent. It is this nearly ideal time behaviour that gives P_2 its special role.

In a half-space of resistivity ρ, the 'diffusion depth'

$$\delta_{\mathrm{TD}} = \delta/\sqrt{2} = \sqrt{\frac{2\rho t}{\mu_0}} \tag{8}$$

provides a measure of the depth to which a surface change in the EM field will propagate in a time t. In heterogeneous earth the diffusion depth can be used as a measure of the depth of detection by replacing ρ in eq. (8) with an apparent resistivity (Raiche & Gallagher 1985). This measure of the detection depth can be refined by integrating the 'diffusion velocity' ($\partial\delta_{\mathrm{TD}}/\partial t$) to give an 'apparent depth'

$$d_{\mathrm{a}}(t) = \int_0^{\mathrm{t}} \frac{\partial\delta_{\mathrm{TD}}}{\partial t}\, dt \tag{9}$$

(Caldwell & Bibby 1998). An example of the application of this methodology is described in Caldwell *et al.* (1999).

Magnetic field response tensor

For a current source turned on abruptly at $t = 0$, the relationship between the observed (time-varying) horizontal magnetic field components and the current sources can also be written in terms of a tensor relationship between the measured horizontal magnetic field and the uniform half-space DC current density **J** at the same point. That is, we can write

$$\mathbf{H}(t) = \boldsymbol{\xi}(t)\mathbf{J}, \tag{10}$$

where $\mathbf{H}(t)$ is the measured *horizontal* magnetic field and $\boldsymbol{\xi}(t)$ is the 'magnetic field response tensor'. For (infinitesimal) dipole sources, $\boldsymbol{\xi}(t)$ is independent of the source orientation.

The magnetic field response tensor for a dipole source on the surface of a uniform resistivity half-space can be derived from expressions given in Ward & Hohmann (1988). In a polar coordinate system (centred on the source dipoles)

$$\boldsymbol{\xi}(t) = (r/4)\begin{bmatrix} 0 & 2(I_0 + 3I_1) \\ -(I_0 + I_1) & 0 \end{bmatrix}\exp[-r^2/(2\delta^2)], \tag{11}$$

where $I_0(r^2/2\delta^2)$ and $I_1(r^2/2\delta^2)$ are modified Bessel functions of the second kind. The magnetic field response tensor has the dimensions of distance and has an implicit dependence upon the resistivity through the parameter δ (eq. 7). At early times ($t \to 0^+$), or equivalently where the source–receiver offset is much greater than the diffusion depth ($r/\delta_{\mathrm{TD}} \gg 1$), the magnetic field response tensor is linearly proportional to δ and has the simple antidiagonal form

$$\boldsymbol{\xi}(t \to 0^+) = (\delta/\sqrt{\pi})\begin{bmatrix} 0 & 2 \\ -\frac{1}{2} & 0 \end{bmatrix}, \tag{12}$$

reflecting the orthogonality of the electric and magnetic fields in a uniform half-space. This tensor may also be represented by an ellipse that has its major axis oriented radially with respect to the source dipoles.

In the DC limit ($t \to \infty$) or equivalently where the source–receiver offset is much less than the diffusion depth ($r/\delta_{\mathrm{TD}} \ll 1$), the horizontal components of the magnetic field measured on the

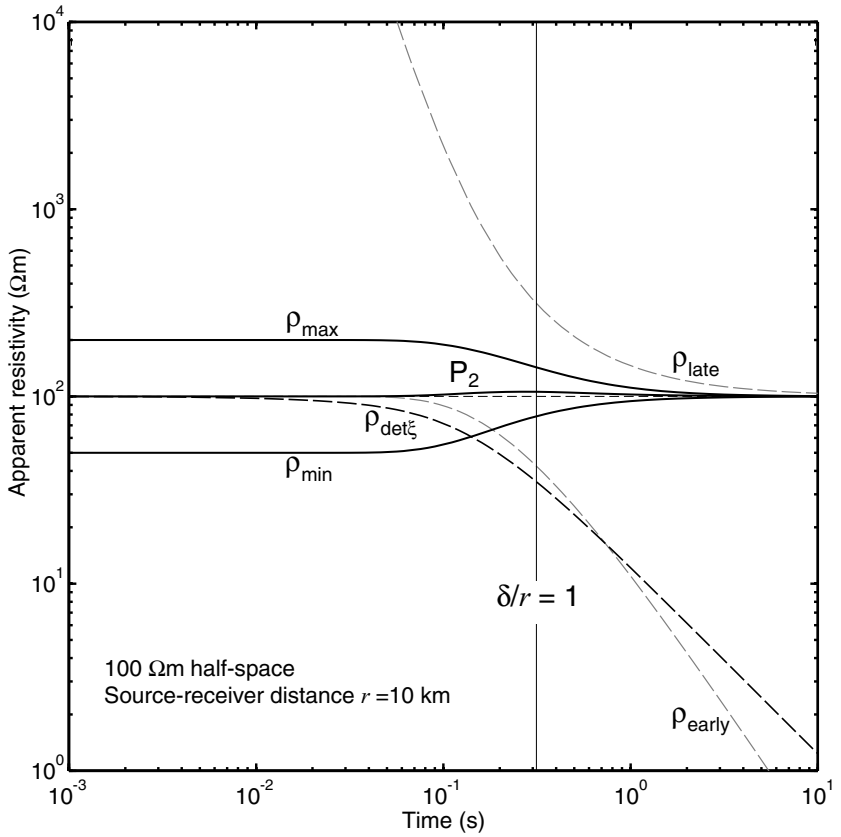

Figure 2. Coordinate-invariant apparent resistivities derived from the instantaneous apparent resistivity tensor (after Caldwell & Bibby 1998). The solid lines show the $\rho_{\max}$, $\rho_{\min}$ and P_2 invariants. The early- and late-time apparent resistivities (ρ_{early} and ρ_{late}) derived from the 'transient part' of the electric field are shown as grey dashed lines. The magnetic field determinant apparent resistivity $\rho_{\det\xi}(t)$ is also shown as dashed line. In a uniform half-space $\rho_{\det\xi}(t)$ is equal to the P_2 apparent resistivity invariant of $\boldsymbol{\rho}_{\mathbf{H}}(t)$.

surface of a homogenous half-space are independent of the resistivity (e.g. Edwards & Nabighan 1991). In this limit the magnetic field response tensor

$$\boldsymbol{\xi}(t \to \infty) = (r/2)\begin{bmatrix} 0 & 1 \\ -\frac{1}{2} & 0 \end{bmatrix} \tag{13}$$

only depends on the distance between the (dipole) sources and the receiver.

Magnetic field apparent resistivity tensor

The half-space behaviour of the magnetic field in the DC limit means that a definition of apparent resistivity based on the magnetic field response tensor is only possible at early times. The relationship between $\boldsymbol{\xi}(t \to 0^+)$ and the half-space resistivity (eq. 12) is quadratic and different definitions of apparent resistivity are possible according to the quadratic function chosen. For example, the determinant of $\boldsymbol{\xi}$ in a uniform half-space at early times

$$\det[\boldsymbol{\xi}(t \to 0^+)] = \delta^2/\pi = 4\rho t/(\mu_0\pi) \tag{14}$$

is linearly proportional to the half-space resistivity and can be used to define a coordinate-invariant magnetic field apparent resistivity:

$$\rho_{\det\xi}(t) = (\mu_0\pi/4t)\det[\boldsymbol{\xi}(t)], \tag{15}$$

which is plotted in Fig. 2. Note that $\rho_{\det\xi}$ is only an accurate measure of the half-space resistivity in the early-time region, i.e. where $r/\delta_{\text{TD}} \gg 1$.

Apparent resistivities can also be derived directly from the squares of the individual components of $\boldsymbol{\xi}(t)$ in the same way that apparent resistivities are formed from the individual components of the MT impedance tensor. However, the matrix of the component apparent resistivities derived in this way does not behave as a tensor when the coordinate system is transformed. To develop an apparent resistivity tensor for the magnetic field we must find a quadratic function of $\boldsymbol{\xi}(t)$ that transforms as a second-rank tensor and, by analogy with the electric field apparent resistivity, has a determinant invariant that gives the resistivity tensor of a uniform half-space at early times. As we show in Appendix A, the tensor given by

$$\boldsymbol{\rho}_{\mathbf{H}}(t) = -(\mu_0\pi/4t)[\text{tr}(\boldsymbol{\xi})\boldsymbol{\xi} - \boldsymbol{\xi}^{\text{t}}\boldsymbol{\xi}], \tag{16}$$

(in matrix notation) has these properties. We will call $\boldsymbol{\rho}_{\mathbf{H}}$ the 'magnetic field apparent resistivity tensor'. This tensor form is (by construction) non-symmetric and has been chosen so that

$$P_2(t) = \{\det[\boldsymbol{\rho}_{\mathbf{H}}(t)]\}^{1/2} = \rho_{\det\xi}(t) \tag{17}$$

in the 3-D case.

The properties of $\boldsymbol{\rho}_{\mathbf{H}}$ can also be described using the concept of an apparent resistivity ellipse. For example, in a polar coordinate system, the early-time form of $\boldsymbol{\rho}_{\mathbf{H}}$ in a uniform half-space of resistivity ρ

$$\boldsymbol{\rho}_{\mathbf{H}}(t \to 0^+) = \begin{bmatrix} \rho_{rr} & \rho_{r\theta} \\ \rho_{\theta r} & \rho_{\theta\theta} \end{bmatrix} = \rho\begin{bmatrix} \frac{1}{4} & 0 \\ 0 & 4 \end{bmatrix} \tag{18}$$

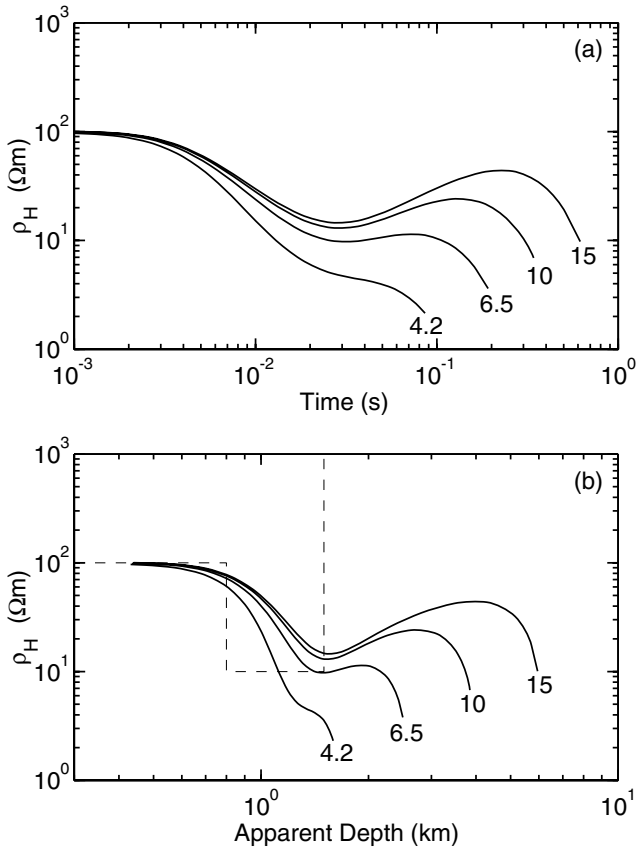

Figure 3. (a) Time-domain magnetic field apparent resistivity sounding curves calculated for a layered half-space at four different locations (source–receiver offsets labelled in km). (b) The same four curves plotted as functions of apparent depth. The dashed line in (b) shows the resistivity depth structure of the layered half-space consisting of 100 and 10 Ω m layers, 0.8 and 0.7 km thick (respectively) overlying a 1000 Ω m substratum.

is similar to the electric field apparent resistivity tensor (eq. 5), the major axis of the apparent resistivity being aligned tangentially with respect to the source dipoles.

Measurements of the magnetic field are usually made with induction coils so that the quantity measured is $-\partial\mathbf{B}/\partial t$ rather than $\mathbf{H}$. However, since $\mathbf{J}$ is independent of time, the same argument used to derive the expressions for the apparent resistivity in eqs (15) and (16) can also be used to express the apparent resistivity directly in terms of the measured quantities $\partial\mathbf{B}/\partial t$. The only differences introduced into eqs (15) and (16) are that the scaling factor changes from $(\mu_0\pi/4t)$ to $(\mu_0\pi t)$ and that the response tensor $\boldsymbol{\xi}$ is replaced by its time derivative $\partial\boldsymbol{\xi}/\partial t$.

Examples of magnetic field apparent resistivity (P_2) sounding curves (computed from calculations of $\partial\mathbf{B}/\partial t$) in a layered half-space are shown in Fig. 3. In contrast to the electric field apparent resistivity P_2, the corresponding magnetic field apparent resistivity reflects the resistivity depth structure only in the early-time region where $r \gg \delta_{\mathrm{TO}}$, i.e. in the time interval before the influence of the source has had time to diffuse outward to reach the measurement site. At late times the apparent resistivity falls to very small values as the induction or 'eddy' currents present at early times decay to insignificant levels. This is reflected in the apparent depth curves (Fig. 3) computed using the P_2 invariant of $\boldsymbol{\rho}_{\mathbf{H}}$ as the measure of resistivity in eq. (9). As can be seen in Fig. 3(b), the apparent depth is effectively limited by the rapid decrease in the apparent resistivity outside the early-time region. This limit depends upon the source–receiver offset and the (unknown) conductivity structure, which will usually be 3-D.

FREQUENCY DOMAIN TENSORS

The grounded source electric and magnetic field (step function) responses in the time domain are usually derived from inverse Laplace transforms of the corresponding frequency-domain *impulse* response functions (e.g. Wait 1961; Ward & Hohmann 1988). Conversely, the frequency-domain tensors (or transfer functions) corresponding to $\boldsymbol{\rho}_{\mathrm{a}}(t)$ and $\boldsymbol{\xi}(t)$ may be derived from the Laplace transform relationships

$$\mathcal{L}[\mathbf{E}(t)] = \hat{\mathbf{E}}(s)/s \tag{19}$$

and

$$\mathcal{L}[\mathbf{H}(t)] = \hat{\mathbf{H}}(s)/s, \tag{20}$$

between the time-domain step function responses $\mathbf{E}(t)$ and $\mathbf{H}(t)$ and the frequency-domain impulse responses $\hat{\mathbf{E}}(s)$ and $\hat{\mathbf{H}}(s)$, where s is the 'complex frequency' and $\mathcal{L}$ is the Laplace transform operator (e.g. Spiegel 1968). Defining the frequency-domain (impulse response) tensors $\hat{\boldsymbol{\rho}}_{\mathrm{a}}(s)$ and $\hat{\boldsymbol{\xi}}(s)$ by the relations

$$\hat{\mathbf{E}}(s) = \hat{\boldsymbol{\rho}}_{\mathrm{a}}(s)\mathbf{J} \tag{21}$$

and

$$\hat{\mathbf{H}}(s) = \hat{\boldsymbol{\xi}}(s)\mathbf{J}, \tag{22}$$

where $\mathbf{J}$ is equal to the DC current density, $\hat{\boldsymbol{\rho}}_{\mathrm{a}}(s)$ and $\hat{\boldsymbol{\xi}}(s)$ are obtained by Laplace transforming the time derivative of the corresponding step function response; i.e.

$$\begin{aligned}\hat{\mathbf{E}}(s) &= s\mathcal{L}[\mathbf{E}(t)] = s\mathcal{L}[\boldsymbol{\rho}_{\mathrm{a}}(t)\mathbf{J}] \\ &= \mathcal{L}[\partial\boldsymbol{\rho}_{\mathrm{a}}(t)/\partial t]\mathbf{J} + \boldsymbol{\rho}_{\mathrm{a}}(t \to 0^+)\mathbf{J}\end{aligned} \tag{23}$$

and

$$\begin{aligned}\hat{\mathbf{H}}(s) &= s\mathcal{L}[\mathbf{H}(t)] = s\mathcal{L}[\boldsymbol{\xi}(t)\mathbf{J}] \\ &= \mathcal{L}[\partial\boldsymbol{\xi}(t)/\partial t]\mathbf{J} + \boldsymbol{\xi}(t \to 0^+)\mathbf{J},\end{aligned} \tag{24}$$

where the integration constants $\boldsymbol{\rho}_{\mathrm{a}}(t \to 0^+)$ and $\boldsymbol{\xi}(t \to 0^+)$ represent the effect of the impulse in the time derivative at $t = 0$ (e.g. Spiegel 1968). Thus

$$\hat{\boldsymbol{\rho}}_{\mathrm{a}}(s) = \mathcal{L}[\partial\boldsymbol{\rho}_{\mathrm{a}}(t)/\partial t] + \boldsymbol{\rho}_{\mathrm{a}}(t \to 0^+) \tag{25}$$

and

$$\hat{\boldsymbol{\xi}}(s) = \mathcal{L}[\partial\boldsymbol{\xi}(t)/\partial t] + \boldsymbol{\xi}(t \to 0^+). \tag{26}$$

The integration constant $\boldsymbol{\rho}_{\mathrm{a}}(t \to 0^+)\mathbf{J}$ on the right-hand side of eq. (23) has a simple physical interpretation. This term represents the electric field produced by the current induced at the Earth's surface by the abrupt change in the time derivative of the magnetic field in the insulating half-space above the Earth. Thus, on the timescales used in TDEM (where we can neglect displacement currents), the electric field or corresponding apparent resistivity is discontinuous at the instant $t = 0$ when the current is turned on (or off) at the source. In contrast, the corresponding term $\boldsymbol{\xi}(t \to 0^+)\mathbf{J}$ for the horizontal magnetic field response (eq. 24) is zero and the horizontal magnetic field will be continuous at $t = 0$. However, $\partial\mathbf{H}(t)/\partial t$, and hence $\partial\boldsymbol{\xi}(t)/\partial t$, will be discontinuous at this point.

For a harmonic excitation (i.e. where $\mathbf{J} = \mathbf{J}^{\mathrm{DC}}\mathrm{e}^{i\omega t}$) we can make the substitution $s = i\omega$, where $\omega = 2\pi/T$ is the angular frequency

and T is the period, and write the frequency-domain impulse response tensors in terms of the frequency ω. Hereafter we will drop the circumflex (ˆ), which we have used to distinguish the impulse response from that of the step response.

Electric field apparent resistivity tensor

In a half-space with uniform resistivity ρ the frequency-domain apparent resistivity tensor in polar coordinates is given by

$$\boldsymbol{\rho}_{\mathrm{a}}(\omega) = \rho \begin{bmatrix} 1 - g(ikr)/2 & 0 \\ 0 & 1 + g(ikr) \end{bmatrix}, \tag{27}$$

where

$$k = (-i\mu_0\omega/\rho)^{1/2} \tag{28}$$

is the wavenumber in a uniform half-space and

$$g(ikr) = [1 - (ikr + 1)\mathrm{e}^{-ikr}] \tag{29}$$

is the frequency-domain impulse response function equivalent to the step function response $f(r/\delta)$ in the time domain, i.e.

$$f(r/\delta) = \mathcal{L}^{-1}[g(s)/s] \tag{30}$$

(e.g. Kaufman & Keller 1983; Ward & Hohmann 1988). The short-period ($T \to 0$ or $\omega \to \infty$) and long period ($T \to \infty$ or $\omega \to 0$) limits are given by

$$\boldsymbol{\rho}_{\mathrm{a}}(\omega \to \infty) = \rho \begin{bmatrix} \frac{1}{2} & 0 \\ 0 & 2 \end{bmatrix} \tag{31}$$

and

$$\boldsymbol{\rho}_{\mathrm{a}}(\omega \to 0) = \rho \begin{bmatrix} 1 & 0 \\ 0 & 1 \end{bmatrix}, \tag{32}$$

which have the same forms as the corresponding time-domain limits (Caldwell & Bibby 1998). Although $\boldsymbol{\rho}_{\mathrm{a}}(\omega)$ is complex in the general case, in these two limits $\boldsymbol{\rho}_{\mathrm{a}}(\omega)$ is real and the measured electric field is in phase with the source current.

Coordinate invariants of complex tensors

Like the MT impedance tensor the frequency-domain apparent resistivity tensor is complex. This makes its representation in terms of coordinate invariants more complicated than in the time domain. In general, $\boldsymbol{\rho}_{\mathrm{a}}(\omega)$ will have four independent complex components that express the magnitude and phase relationship between the measured electric field vector and the uniform half-space current density **J** representing the current source. Physically, this is an expression of the elliptically polarized electric field that is produced by a grounded source when the conductivity distribution is 3-D.

The real and imaginary parts of $\boldsymbol{\rho}_{\mathrm{a}}(\omega)$ are non-symmetric tensors in their own right (although related by a Hilbert transform) with each part of the tensor having three coordinate invariants, which may each be represented by an ellipse. Thus any complex frequency second-rank tensor may be represented graphically as a pair of ellipses. A seventh 'mixed' invariant links the two parts of the tensor as Szarka & Menvielle (1997) have pointed out for the MT impedance tensor. This invariant has a simple geometrical interpretation in terms of the ellipse pair representing the complex tensor and is most easily thought of as the angle between the major axes of the ellipses. The ellipse axes will be parallel only in situations with a high degree of symmetry, e.g. where the conductivity structure is 1-D. The single coordinate-dependent parameter needed to complete the description of the complex tensor can be taken to be the orientation of the major axis of one of the ellipses.

Transforming from the time-domain to the frequency-domain implicitly includes information concerning the rate of change of the time-domain tensor. It is this information that gives rise to the 'extra' four invariants found in the frequency-domain form of the tensor.

Although other graphical representations of the invariants of complex (frequency-domain) tensors are possible (Szarka & Menvielle 1997; Weaver *et al.* 2000), we will describe the coordinate invariants of the apparent resistivity tensor in terms of properties of the ellipses representing the real or 'in-phase' and the imaginary or 'quadrature' parts of the tensor with two exceptions discussed later. Using this representation we are able to visualize the apparent resistivity tensor in a way that reflects the underlying conductivity distribution and apply the techniques developed for the time-domain apparent resistivity tensor (Caldwell & Bibby 1998).

In the discussion that follows we will specify which part of the tensor we are dealing with in the subscript of the invariant concerned. For example, we will write the invariants of the real and imaginary tensors corresponding to P_2 as

$$P_{\Re 2} = \det(\Re[\boldsymbol{\rho}_{\mathrm{a}}(\omega)])^{1/2} \tag{33}$$

and

$$P_{\Im 2} = \det(\Im[\boldsymbol{\rho}_{\mathrm{a}}(\omega)])^{1/2}. \tag{34}$$

We will also use the 'mixed' invariant given by the magnitude of the determinant of the complex tensor

$$\rho_{\det} = |\det[\boldsymbol{\rho}_{\mathrm{a}}(\omega)]|^{1/2}, \tag{35}$$

which is a function of all seven invariant parameters described above. Various coordinate-invariant 'phases' can also be defined from ratios of the real and imaginary tensor invariants. In particular, we will show examples of the phases given by the ratios of the determinant invariants

$$\Phi_0 = \frac{1}{2}\arctan\{\Im(\det[\boldsymbol{\rho}_{\mathrm{a}}(\omega)])/\Re(\det[\boldsymbol{\rho}_{\mathrm{a}}(\omega)])\} \tag{36}$$

(another mixed invariant) and

$$\Phi_2 = \frac{1}{2}\arctan\{\det(\Im[\boldsymbol{\rho}_{\mathrm{a}}(\omega)])/\det(\Re[\boldsymbol{\rho}_{\mathrm{a}}(\omega)])\}, \tag{37}$$

the latter being a measure of the relative areas of the ellipses representing the in-phase and quadrature tensors.

Electric field apparent resistivity tensor invariants

Apparent resistivity and phase invariants for a uniform half-space are shown in Fig. 4. At short periods ($\omega \to \infty$), $\rho_{\Re\,\min}$ and $\rho_{\Re\,\max}$ are radial and tangential to the source dipoles, respectively, and have the same values ($\rho/2$ and 2ρ) as their time-domain equivalents (Fig. 2). At long periods ($\omega \to 0$), $\rho_{\Re\,\min}$ and $\rho_{\Re\,\max}$ converge to the half-space resistivity. The invariants $P_{\Re 2}$ and $\rho_{\det}$ are well behaved, deviating from the half-space value by no more than 6 and 12 per cent, respectively. The coordinate-invariant phases (Φ_2 and Φ_0) corresponding to $P_{\Re 2}$ and $\rho_{\det}$ are also well behaved, deviating from zero by less than 4° and 6°, respectively. The corresponding invariants for the quadrature tensor (Fig. 4b) vanish at short and long periods, where the electric field is in phase with the source current and are significant only in the region where the source–receiver offset becomes comparable to the 'skin depth',

$$\hat{\delta} = [2\rho/(\mu_0\omega)]^{1/2}. \tag{38}$$

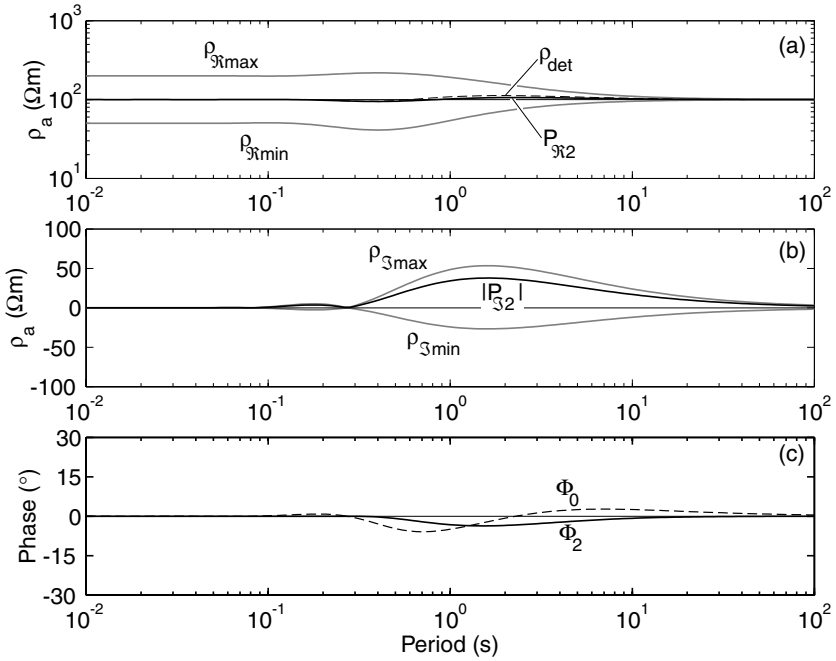

Figure 4. Frequency-domain apparent resistivities and phase invariants for the electric field apparent resistivity tensor in a uniform 100 Ω m half-space. The source–receiver offset is 10 km. (a) Log–log plots of the $P_{\Re 2}$, $\rho_{\Re\,\min}$ and $\rho_{\Re\,\max}$ apparent resistivity invariants. The determinant apparent resistivity $\rho_{\det}$ is also shown, although it is virtually indistinguishable from $P_{\Re 2}$. (b) The corresponding imaginary (or quadrature) tensor invariants $|P_{\Im 2}|$, $\rho_{\Im\,\min}$ and $\rho_{\Im\,\max}$ (note that the apparent resistivity scale is linear). (c) Coordinate-invariant phases Φ_0 (dashed line) and Φ_2.

Since the apparent resistivity tensor is symmetric in a uniform (or indeed in a 1-D) half-space it is characterized by the lengths of the two sets of ellipse axes and by the orientations of the ellipse axes with respect to the source dipoles. For a uniform half-space the ellipse representing the in-phase part of the tensor is oriented tangentially at early times and becomes circular in the DC limit. The behaviour of the quadrature tensor (Fig. 4b) is more complicated, the tensor ellipse changing from a radial to a tangential orientation at ∼0.3 s, where $\rho_{\Im\,\min}$ and the quadrature tensor determinant become negative.

While it is not surprising that the quadrature part of the apparent resistivity tensor may have a negative determinant we would not normally expect the in-phase part of the electric field apparent resistivity tensor to have a negative determinant except in cases where the conductivity distribution is very unusual. Thus, it should not be assumed that either the electric or magnetic field apparent resistivity tensors are *necessarily* 'positive definite', especially where the conductivity structure is 3-D. However, a measurement that produces a negative value of $\det[\Re(\boldsymbol{\rho}_{\rm a})]$ should be treated with caution as in most (though not all) cases it will be a sign of a problem with the measurement rather than an unusual conductivity distribution.

Examples of the frequency-domain apparent resistivity ($P_{\Re 2}$) and phase (Φ_0) sounding curves for a horizontally layered half-space are shown in Fig. 5. The in-phase sounding curves are similar to the corresponding time-domain soundings discussed in (Caldwell & Bibby 1998) and reflect the resistivity depth structure until the DC limit is approached. The phase Φ_0 is also well behaved and reflects (imperfectly) the negative gradient of the sounding curve. Using $P_{\Re 2}(\omega)$ as the measure of resistivity, it is possible to derive the frequency domain equivalent to the time-domain apparent depth (eq. 9) by integrating $\partial\hat{\delta}/\partial T$ as a function of period. We define the frequency-domain apparent depth as

$$d_{\rm a}(\omega) = \frac{1}{\sqrt{2}} \int_0^{\rm T} \frac{\partial \hat{\delta}}{\partial T}\, dT, \tag{39}$$

where the $1/\sqrt{2}$ scaling factor has been chosen so that the apparent resistivity of a layered half-space first begins to fall or rise at an apparent depth approximately equal to the thickness of the uppermost layer in a similar way to the time-domain case. The apparent depth curves (Fig. 5c) allow us to compare frequency-domain apparent resistivity sounding curves with the resistivity depth structure in the same way as is possible for time-domain or DC resistivity sounding.

The magnetic field response tensor

In polar coordinates, the frequency-domain magnetic field response tensor in a uniform half-space is given by

$$\boldsymbol{\xi}(\omega) = r/2 \begin{bmatrix} 0 & ikr(I_0K_1 - K_0I_1) - 6I_1K_1 \\ I_1K_1 & 0 \end{bmatrix}, \tag{40}$$

where $K_0(ikr/2)$, $K_1(ikr/2)$, $I_0(ikr/2)$ and $I_1(ikr/2)$ are modified Bessel functions of the first and second kind. At short periods (i.e. $\omega \to \infty$ or $r/\hat{\delta} \gg 1$), equivalent to the early-time region in the time domain,

$$\boldsymbol{\xi}(\omega \to \infty) = (1-i)\hat{\delta}/2 \begin{bmatrix} 0 & 2 \\ -\frac{1}{2} & 0 \end{bmatrix}. \tag{41}$$

Thus, if the source–receiver offset is much greater than the skin-depth ($r/\hat{\delta} \gg 1$), $\boldsymbol{\xi}(\omega)$ has a $\pm 45^\circ$ phase difference with respect to **J** and has the same square root time and resistivity dependence as its time-domain counterpart. The off-diagonal form of $\boldsymbol{\xi}(\omega)$ in a uniform half-space reflects the orthogonality of the horizontal electric and magnetic field. We can also represent the complex tensor $\boldsymbol{\xi}$ as a pair of ellipses. However, in contrast to the electric field

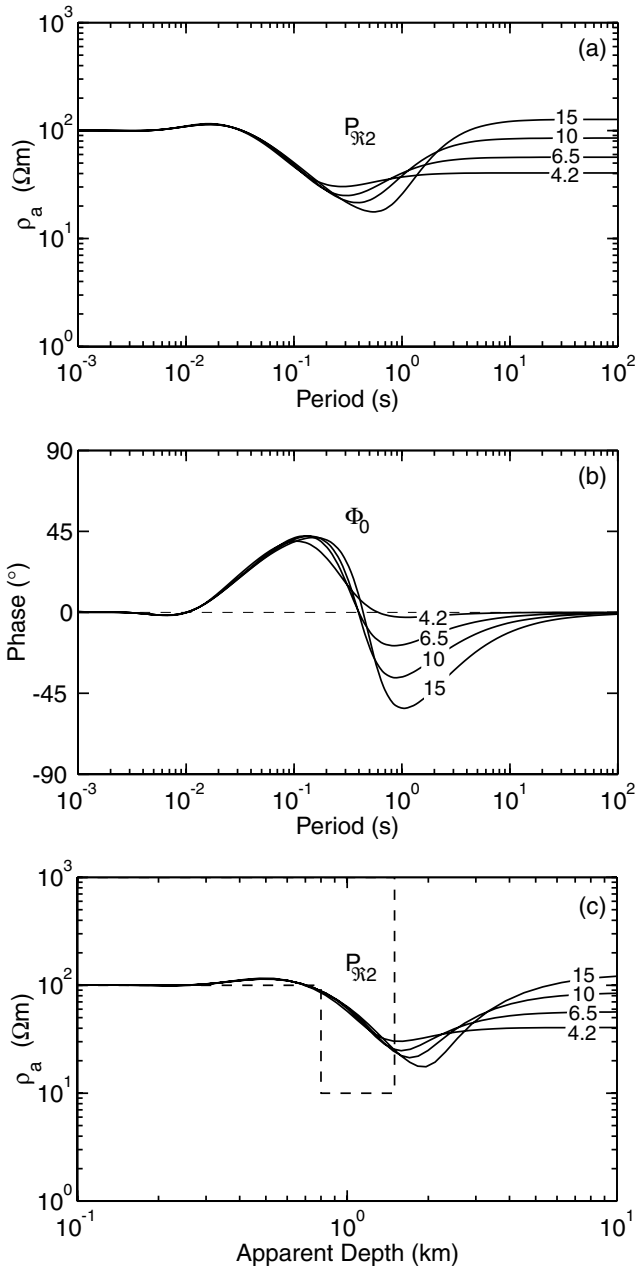

Figure 5. Frequency-domain electric field sounding curves for the same layer model and source–receiver offsets as used in Fig. 3: (a) in-phase apparent resistivity, (b) coordinate-invariant phase and (c) the in-phase apparent resistivity plotted as a function of apparent depth. The dashed line in (c) shows the resistivity depth structure of the layer model.

apparent resistivity, the major axes of the ellipses representing $\boldsymbol{\xi}$ are oriented radially with respect to the source dipoles rather than tangentially.

At long periods (i.e. as $\omega \to 0$ or as $r/\hat{\delta} \ll 1$) the magnetic field is in phase with the source current and $\boldsymbol{\xi}(\omega)$ has the same form as the DC (or late-time) limit of $\boldsymbol{\xi}(t)$ (eq. 13); i.e. $\boldsymbol{\xi}(\omega)$ is independent of period and resistivity but linearly proportional to distance.

The magnetic field apparent resistivity tensor

Scalar apparent resistivities can be formed from quadratic functions of $\boldsymbol{\xi}(\omega)$ in the same way as in the time domain. Taking the determinant of $\boldsymbol{\xi}(\omega)$ in eq. (41), we can see that the (complex) apparent resistivity

$$\rho_{\det \xi}(\omega) = i\omega\mu_0 \det[\boldsymbol{\xi}(\omega)] \tag{42}$$

has the value of the half-space resistivity as $T \to 0$ (i.e. $\omega \to \infty$). A frequency-domain 'magnetic field apparent resistivity tensor' $\boldsymbol{\rho}_{\mathbf{H}}(\omega)$ may be defined in the same way as for the time domain (Appendix A), i.e.

$$\boldsymbol{\rho}_{\mathbf{H}}(\omega) = -i\omega\mu_0[\mathrm{tr}(\boldsymbol{\xi})\boldsymbol{\xi} - \boldsymbol{\xi}^{\mathrm{t}}\boldsymbol{\xi}]. \tag{43}$$

In the short-period limit $\boldsymbol{\rho}_{\mathbf{H}}(\omega)$ takes the form of the resistivity tensor of the half-space as we require.

Fig. 6 shows the frequency-domain magnetic field apparent resistivity and phases corresponding to those shown in Fig. 4 for the electric field response. Note that the uniform half-space properties of $\rho_{\det \xi}$ in the frequency domain (Fig. 6) are similar to those of $\rho_{\det \xi}$ in the time domain (Fig. 2), the major difference being the small 'overshoot' present in the frequency-domain response before the apparent resistivity 'rolls off' at long periods. Compared with the corresponding invariants for the electric field (Fig. 4) the

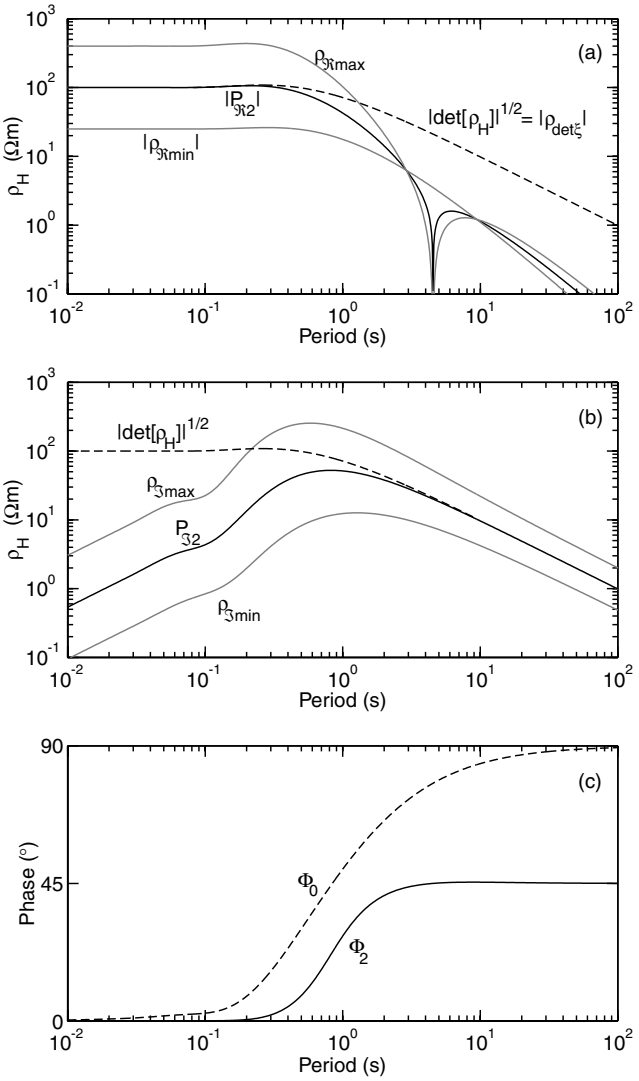

Figure 6. Frequency-domain magnetic field sounding curves for a 100 Ω m half-space at a source–receiver offset of 10 km: (a) in-phase apparent resistivity, (b) quadrature apparent resistivity and (c) phase coordinate invariants.

magnetic field response is more complicated. In particular, $\rho_{\Re\,\min}$ and the determinant of $\boldsymbol{\rho}_{\mathbf{H}}$ become negative for periods greater than ~4.5 s. The magnitudes of the corresponding apparent resistivities are plotted in Fig. 6.

At short periods the major axis of the in-phase ellipse ($\rho_{\Re\,\max}$) is oriented tangentially. As the response begins to roll off with increasing period, the major axis of the ellipse shrinks more rapidly than the minor axis and the ellipse becomes circular at the point where all three invariants plotted in Fig. 6(a) intersect. As the period continues to increase, the major axes flips into the radial direction while the minor axes (now oriented tangentially) decrease even more rapidly, eventually becoming zero at which point the area of the ellipse and thus $P_{\Re 2}$ are also zero. At this point the in-phase horizontal magnetic field is linearly polarized in the radial direction. At still longer periods the minor axes redevelops, increasing until the ellipse becomes circular again whereupon the major axis flips back into the tangential direction and takes on its DC form, with the major axis being four times the length of the minor axes.

Fig. 7 shows the magnetic field apparent resistivity, phase and apparent depth curves corresponding to those shown in Fig. 5 for the electric field. As expected the depth structure of the resistivity is only reflected in the magnetic field response at short periods (i.e. $r \gg \hat{\delta}$). This will also be true in a 3-D situation. However, in a 3-D situation the period range over which $\boldsymbol{\rho}_{\mathbf{H}}$ will be representative of the subsurface resistivity will depend on the conductivity structure in a complicated way. Thus, as is the case in a CSMT survey, the magnetic field apparent resistivity may be misleading at longer periods where the source effects begin to become important.

The CSMT impedance tensor

Where the source–receiver distance is much greater than the skin depth, the EM field at the surface can be considered to be a vertically incident plane wave and the 'magnetotelluric approximation' will apply. In this situation (i.e. as $T \to 0$ or as $r \gg \hat{\delta}$), the subsurface conductivity structure can be inferred from local measurements of the electric and magnetic fields as a function of frequency without reference to the source. At a given measurement location this information is expressed in the impedance tensor $\mathbf{Z}(\omega)$, which is defined by the tensor relation

$$\mathbf{E}(\omega) = \mathbf{Z}(\omega)\mathbf{H}(\omega). \tag{44}$$

For CSMT this relationship (eq. 44) may also be expressed in terms of the frequency-domain response tensors corresponding to **E** and **H** (eqs 21 and 22), i.e.

$$\mathbf{E}(\omega) = \boldsymbol{\rho}_{\mathrm{a}}(\omega)\mathbf{J} = \mathbf{Z}(\omega)\boldsymbol{\xi}(\omega)\mathbf{J}. \tag{45}$$

Eliminating **J**, which represents the source information in eq. (45), the CSMT impedance tensor is given by

$$\mathbf{Z}(\omega) = \boldsymbol{\rho}_{\mathrm{a}}(\omega)[\boldsymbol{\xi}(\omega)]^{-1}, \tag{46}$$

which has a similar form to an expression given by Li & Pedersen (1991). In the short-period limit ($\omega \to \infty$ or $r \gg \hat{\delta}$) the CSMT impedance tensor in a uniform half-space can be derived directly from the corresponding forms of $\boldsymbol{\rho}_{\mathrm{a}}(\omega)$ and $\boldsymbol{\xi}(\omega)$ (eqs 35 and 45) in a polar coordinate system and

$$\mathbf{Z}(\omega \to \infty) = \boldsymbol{\rho}_{\mathrm{a}}\boldsymbol{\xi}^{-1} = (i\mu_0\omega\rho)^{1/2}\begin{bmatrix} 0 & -1 \\ 1 & 0 \end{bmatrix}. \tag{47}$$

The CSMT impedance tensor in the DC limit (also given in Li & Pedersen 1991)

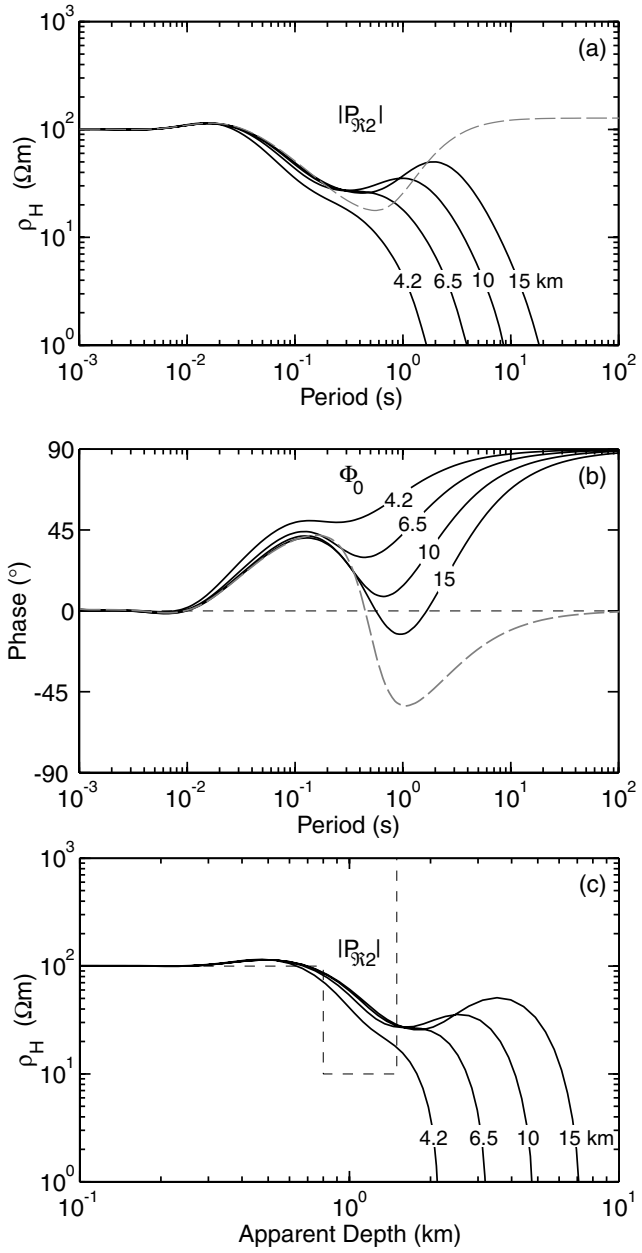

Figure 7. Magnetic field sounding curves for the same layered model and source–receiver offsets as used in Figs 3 and 5: (a) in-phase apparent resistivity, (b) coordinate-invariant phase and (c) the in-phase apparent resistivity plotted as a function of apparent depth. For comparison, the corresponding electric field apparent resistivity (a) and phase (b) at a source–receiver offset of 15 km are shown as grey dashed lines. The dashed line in (c) shows the resistivity depth structure of the layer model.

$$\mathbf{Z}(\omega \to 0) = (2\rho/r)\begin{bmatrix} 0 & -2 \\ 1 & 0 \end{bmatrix} \tag{48}$$

can be derived directly from the corresponding DC limits of $\boldsymbol{\rho}_{\mathrm{a}}$ and $\boldsymbol{\xi}$ (eqs 32 and 13). In this limit the CSMT impedance tensor is explicitly source dependent since the tensor is inversely proportional to the source–receiver offset. Note that the source dependence enters through the magnetic field response tensor $\boldsymbol{\xi}$.

In CSMT, the plane wave approximation breaks down in the region where the source–receiver distance becomes comparable to

the skin depth (i.e. $r \rightarrow \hat{\delta}$) and the magnetic field starts to become independent of the conductivity. This effect causes the MT apparent resistivity to rise unrealistically as the magnitude of ξ falls to very small values. The EM field observations still contain information concerning the conductivity structure but the information is contained in the electric field (i.e. in ρ_a) rather than in the horizontal magnetic field components (Routh & Oldenburg 1999) or ξ. The frequency range over which the MT approximation is valid depends upon the resistivity structure under investigation (e.g. Wannamaker 1997), something that is unknown *a priori*. This introduces a degree of ambiguity into the interpretation of CSMT data that can only be avoided by including source information into the analysis.

3-D EFFECTS

A coordinate-invariant approach to EM data analysis is most useful when the conductivity distribution is 3-D. In this situation there is no preferred or natural frame of reference and the response will depend upon the polarization of the EM field in a way that depends on the conductivity structure. We will illustrate the properties of the electric and magnetic field apparent resistivity tensors using two of the models that we used in our study of the time-domain electric field apparent resistivity tensor (Caldwell & Bibby 1998). The model results discussed in the following sections were all calculated using the 3-D integral equation modelling code described in Xiong (1992) and in Xiong & Tripp (1995).

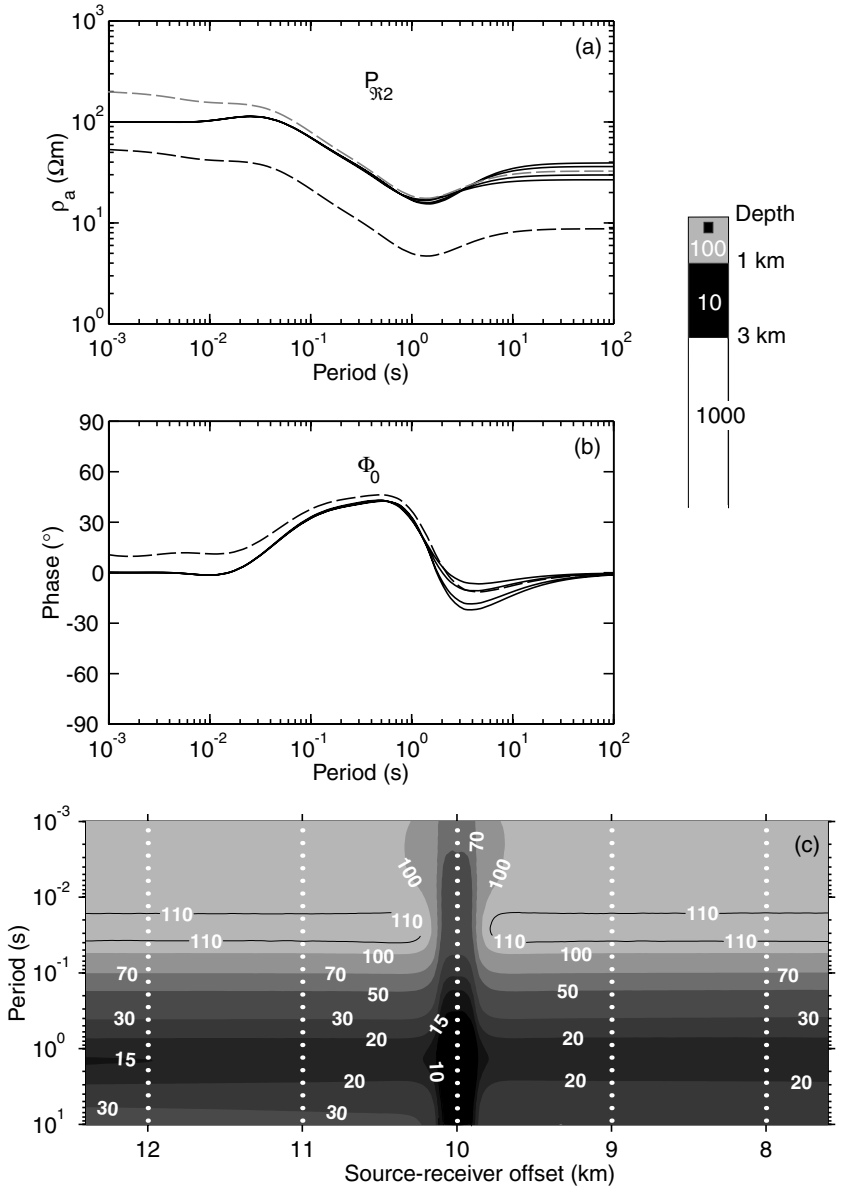

Figure 8. (a) Electric field apparent resistivity ($P_{\Re 2}$) sounding curves in the frequency domain for the three layer model depicted to the right of the sounding curves. The model consists a 10 Ω m cube (0.25^3 km^3) embedded in the top (100 Ω m) layer. The upper surface of the cube is 25 m below the surface. The black dashed line shows the apparent resistivity at a point located above the centre of the cube where the source–receiver offset is 10 km. The grey dashed line shows the same sounding curve displaced vertically upwards so that the apparent resistivity at $T = 100$ s matches the DC apparent resistivity of a layered half-space at the same source–receiver offset (i.e. in the absence of the cube). (b) Corresponding coordinate-invariant phase (Φ_0) sounding curves. (c) Electric field apparent resistivity ($P_{\Re 2}$) pseudo-section (computed at sites 50 m apart) along a line crossing over the centre of the cube. The vertical columns of white dots on the pseudo-section show the locations of the sounding curves shown in (a) and (b).

Static effects

After an initial period, during which time the eddy currents induced within and around a small near-surface heterogeneity are significant, the 'anomalous' electric field produced by galvanic effects (charges) at the boundaries of the heterogeneity reaches a steady state and is virtually independent of time. Equivalently, in the frequency domain, the phase of the anomalous electric field is independent of the source frequency at long periods. The effects of the boundary charges, known as 'static effects' in MT surveys (see Jiracek 1990 for a review), have been discussed by Zonge & Hughes (1991) and Qian & Pedersen (1992) for CSMT measurements. The corresponding effect on the time-domain apparent resistivity tensor was discussed in Caldwell & Bibby (1998) and has also been discussed by Newman (1989) and Strack (1992) for deep transient EM soundings using single sources.

If the 'underlying' electric field (i.e. the electric field in the absence of the heterogeneity) does not change significantly over the extent of the heterogeneity, the 'scattered' or 'anomalous' electric field is (to a good approximation) linearly dependent on the underlying electric field (e.g. Chave & Smith 1994). In this case the total electric field is well approximated by the sum of the scattered and underlying fields. Thus from eq. (1), for a time $t > t_{\text{static}}$ or period $T > T_{\text{static}}$, the observed or 'distorted' (electric field) apparent resistivity tensor $\tilde{\boldsymbol{\rho}}_{\text{a}}$ is given by

$$\tilde{\boldsymbol{\rho}}_{\text{a}} = (\mathbf{I} + \mathbf{D})\boldsymbol{\rho}_{\text{a}}, \tag{49}$$

where $\mathbf{I}$ is the identity matrix, $\mathbf{D}$ is the distortion matrix (a 2×2 real matrix that is independent of time or frequency) and $\boldsymbol{\rho}_{\text{a}}$ is the matrix representing the underlying apparent resistivity tensor, i.e. the tensor that would be measured in the absence of the heterogeneity.

Since the determinant of a matrix product is the product of the individual matrix determinants

$$\det(\tilde{\boldsymbol{\rho}}_{\mathbf{a}}) = \det[(\mathbf{I} + \mathbf{D})\boldsymbol{\rho}_{\text{a}}] = \det(\mathbf{I} + \mathbf{D})\det(\boldsymbol{\rho}_{\text{a}}) \tag{50}$$

the observed invariant $\tilde{P}_2$ in either the time or frequency domain will be scaled by a constant factor with respect to the underlying value of P_2.

In the time domain, an apparent resistivity sounding curve (i.e. log–log plots of P_2 versus time) measured near a localized heterogeneity will be offset along the apparent resistivity axis with respect to an undistorted sounding curve in the same way as a MT apparent resistivity sounding curve, which is said to be 'statically shifted'. However, the gradient of the time-domain sounding curve, $\partial \log(P_2)/\partial \log(t)$ will be virtually unaffected by the heterogeneity (Caldwell & Bibby 1998).

In the frequency domain, the effect of the heterogeneity as expressed by eq. (49) is the same on the real and imaginary parts of the tensor. Thus $P_{\Re 2}(\omega)$ and $P_{\Im 2}(\omega)$ are scaled in the same way as the corresponding time-domain invariant and the ratio of the in-phase and quadrature ellipse areas is unchanged, i.e.

$$\begin{aligned}\tan(2\Phi_2) &= \det(\Im[\tilde{\boldsymbol{\rho}}_{\mathbf{a}}])/\det(\Re[\tilde{\boldsymbol{\rho}}_{\mathbf{a}}]) \\ &= \det(\Im[\boldsymbol{\rho}_{\text{a}}])/\det(\Re[\boldsymbol{\rho}_{\text{a}}])\end{aligned} \tag{51}$$

and the phase Φ_2 will be unaffected by the heterogeneity. The relationship given in eq. (50) also applies to a complex tensor and thus we also expect the phase Φ_0 to be unaffected.

In general, the heterogeneity will distort the underlying apparent resistivity tensor into a 3-D form in a way that will depend on the geometry of heterogeneity and the position of the receiver. Without other information or assumptions concerning the nature of the underlying apparent resistivity tensor the magnitude of the scale-factor $\det([\mathbf{I} + \mathbf{D}])$ and the structure of the distortion matrix are not determinable, as is the case in MT.

Static shift model

The effects produced in frequency-domain electric field apparent resistivity sounding curves by a small conductive cube embedded in the surface layer of a layered half-space are shown in Fig. 8. For the site located immediately above the conductive cube (at a source–receiver offset of 10 km (Fig. 8a) the apparent resistivity ($P_{\Re 2}$) sounding curve is shifted as expected. As can be seen in the apparent resistivity pseudo-section (Fig. 8c) and the apparent resistivity ellipse map (Fig. 9) the effects of the heterogeneity on the $P_{\Re 2}$ invariant are confined to a small area in the immediate vicinity of the cube. The 3-D nature of the distortion is shown in Fig. 9 by the variation of the ellipse axes directions near the cube. At periods less than $\sim$1 s, the invariant phases, Fig. 8(b), from the undistorted sites surrounding the conductive cube are essentially the same. In this period range, the phase from the distorted site above the cube is shifted by a small amount with respect to the undistorted curves, the phase shift decreasing slowly as the period increases.

The effect of the localized near-surface heterogeneity on the horizontal magnetic field is much smaller than the corresponding effect on the electric field as shown in Fig. 10. Although the effect of the eddy currents 'trapped' within the conductive cube can be seen at short periods in the area above the cube, the magnitude of the magnetic field apparent resistivity reflects the underlying layered structure and is almost totally insensitive to the presence of the cube. At still longer periods, where the source–receiver offset becomes

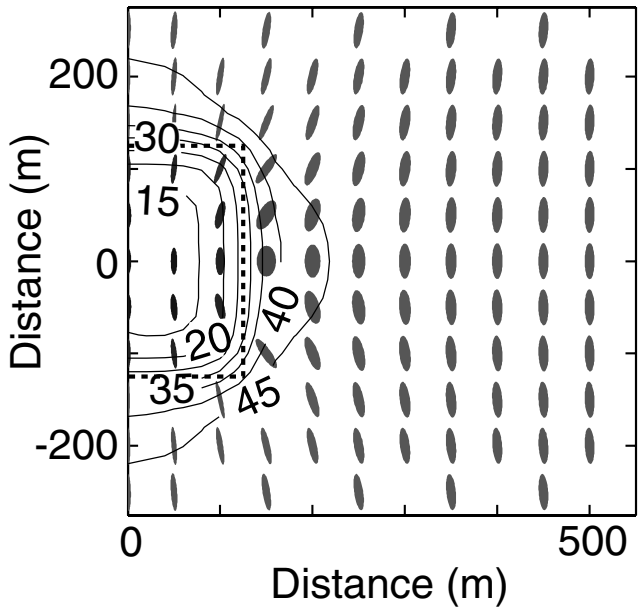

Figure 9. Frequency-domain (electric field) apparent resistivity ellipse map at $T = 0.2$ s for the conductivity model shown in Fig. 8. The outline of the right-hand half of the conductive (10 Ω m) cube is shown by the dashed line. The current sources (not shown) lie 10 km to the right of the centre of the cube along the x-axis. The apparent resistivity ellipses represent the in-phase part of the apparent resistivity tensor i.e. $\Re[\boldsymbol{\rho}(\omega)]$. The contours show the value of the coordinate-invariant apparent resistivity $P_{\Re 2}$ (contour interval of 5 Ω m). The lengths of the ellipse axes have been normalized so that the lengths of the major axis ($\rho_{\Re\,\max}$) are proportional to $\log(\rho_{\Re\,\max})$. For the locations shown in the figure the $P_{\Re 2}$ apparent resistivity of the (background) layered half-space at $T = 0.2$ s is approximately 50 Ω m.

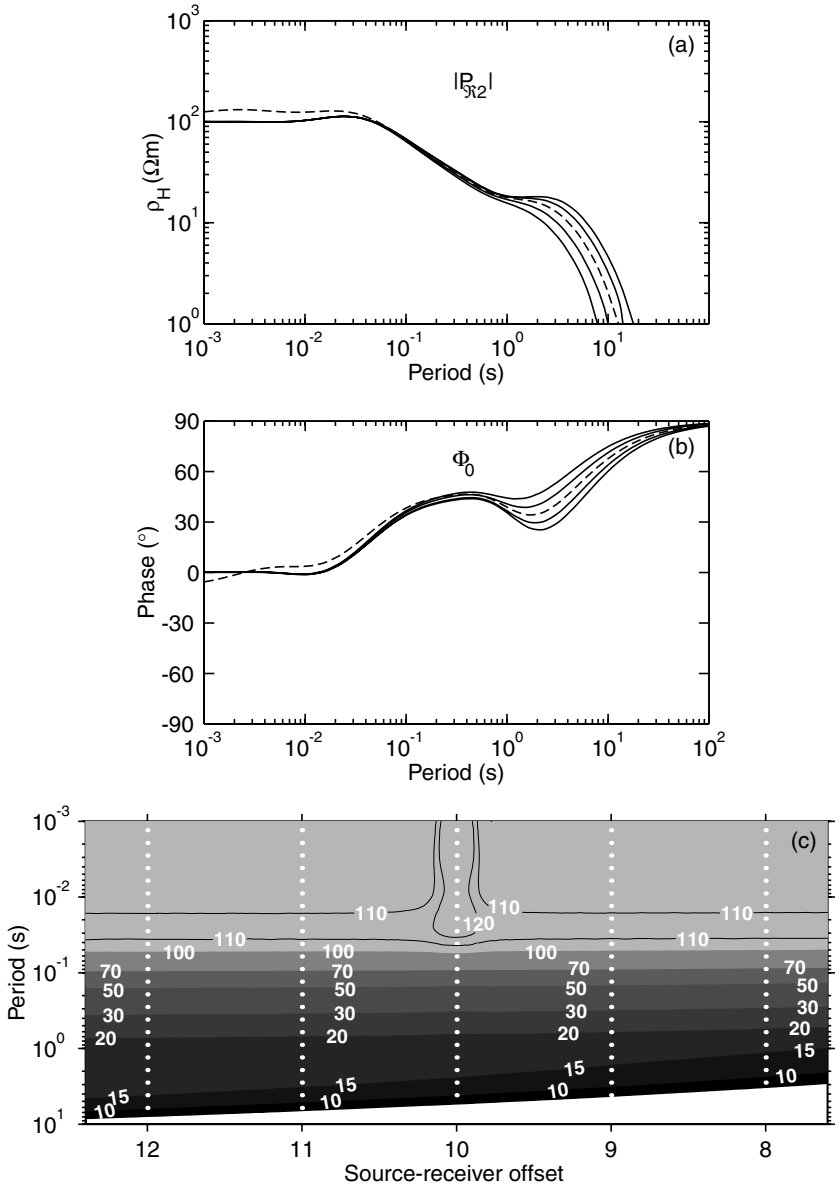

Figure 10. (a) Frequency-domain magnetic field apparent resistivity ($P_{\Re 2}$) sounding curves for the 3-D resistivity model shown in Fig. 8. The dashed line shows the apparent resistivity at a point located above the centre of the conductive cube where the source–receiver offset is 10 km. (b) Corresponding coordinate-invariant phase (Φ_0) sounding curves. (c) Magnetic field apparent resistivity ($P_{\Re 2}$) pseudo-section (computed at sites 50 m apart) along a line crossing over the centre of the cube. The vertical columns of white dots on the pseudo-section show the locations of the sounding curves in (a) and (b). Apparent resistivity values <7 Ω m are not shown on the pseudo-section.

comparable to the skin depth, the magnetic field apparent resistivity becomes unrealistically small. A small phase shift is also present in the magnetic field phase response for periods less than ∼1 s.

Model geothermal system

Fig. 11 shows an idealized model of the conductivity structure typical of the high-temperature geothermal systems found in New Zealand. The deeper, conductive parts of these systems lie beneath a more highly conducting superficial layer produced by the combined effects of hydrothermal alteration, slightly acidic saline pore fluids and elevated temperatures. In the model, we have extended the near-surface conductor laterally to simulate the presence of a subsurface out-flow of geothermal fluid that occurs in geothermal systems both in New Zealand and elsewhere (e.g. Bibby *et al.* 1984). Although the near-surface high-conductivity region can be easily delineated by many different electrical exploration techniques, identifying the deeper conductor (which represents the 'target' high-temperature fluid reservoir useful for electric power production) is much more difficult. Pellerin *et al.* (1996) in their study of this problem concluded that the information concerning the location of the reservoir area would be contained in the electric field. The behaviour of the instantaneous apparent resistivity tensor, representing the time-domain electric field, supports this conclusion (Caldwell & Bibby 1998).

Fig. 12 shows maps of the in-phase electric field apparent resistivity tensor ellipses at three different periods. These maps have been chosen so that the apparent depth is approximately the same

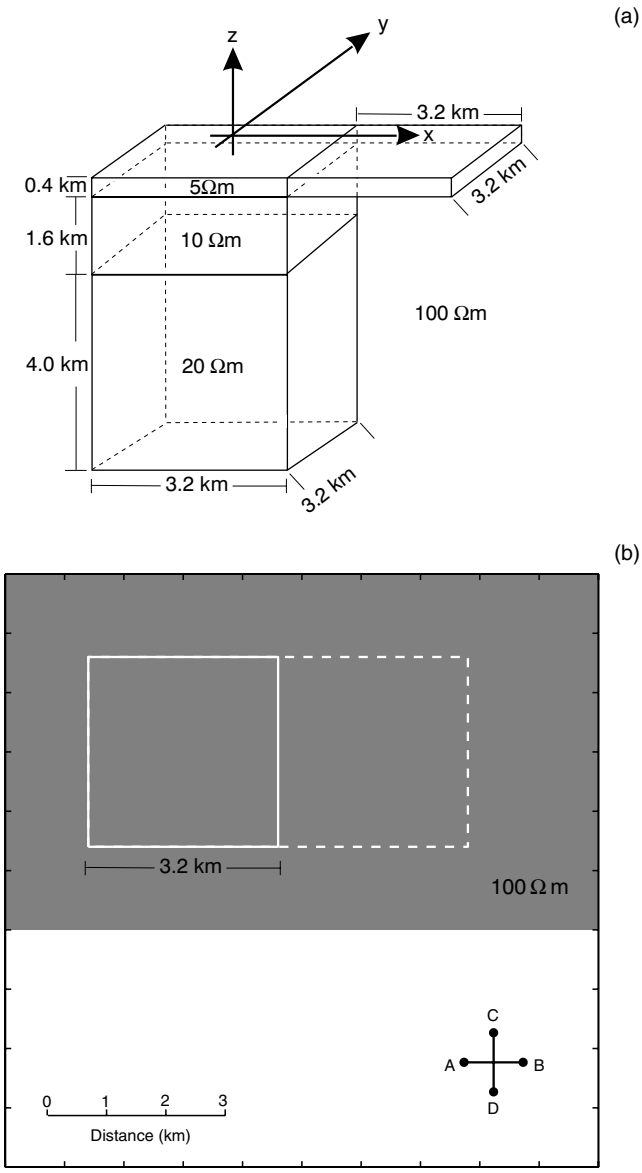

Figure 11. (a) A perspective view of the resistivity model used to compute the tensor ellipse maps shown in Figs 12–14. (b) A map view showing the position of the grounded source bipoles (AB and CD) used for this computation. The grey area shows the region covered by each of the ellipse maps in the following figures. The white line shows the outline of the conductive body, the top part of which is Loom below the surface.

as that of the corresponding time-domain apparent resistivity maps shown in Caldwell & Bibby (1998), which show essentially the same features. At short periods ($T = 0.13$ s) the major axes of the tensor ellipses are aligned tangentially with respect to the source (the location of which is shown in Fig. 11). This tangential alignment of the ellipses reflects the dominantly inductive regime where the skin depth is much less than the source–receiver offset and the surface EM field may be approximated as a plane wave. Where the source–receiver offset is comparable to the skin depth, the galvanic influence of the source becomes more dominant. This can be seen in the lower right-hand corner of the $T = 1.3$ s maps where the ellipse shapes are more nearly circular. At longer periods the effect of the boundary charges become important and the in-phase ellipse alignments change so that the major axes of the ellipses near the edges of the conductive body 'point' towards the body in the same way as the TDEM ellipses do at late times (Caldwell & Bibby 1998). As is also the case in the time domain, the area underlain by the conductive block representing the reservoir is more clearly distinguishable in the minimum apparent resistivity ($\rho_{\Re\,\min}$) than in the $P_{\Re 2}$ invariant maps. The behaviour of the quadrature electric field apparent resistivity tensor (Fig. 13) is not as easily interpretable and the invariant phases Φ_0 and Φ_2 (contours shown in Fig. 13) are more useful parameters. Although the upper part of the conductive body can be seen in both cases, only the Φ_0 map clearly shows the deeper part of the conductive body.

Examples of the in-phase and quadrature magnetic field apparent resistivity ellipses are shown in Fig. 14. As can be seen in the left-hand half of Fig. 14, the conductive body produces only small effects in the in-phase $P_{\Re 2}$ apparent resistivity. At longer periods the effect of the source is marked by the rapid decrease in $P_{\Re 2}$ and by a change in the ellipse orientation from tangential to radial as can be seen in the lower right-hand corner of the $T = 0.6$ s in-phase ellipse map. Although the in-phase tensor hardly senses the conductive body at all, there is a small but distinct response in the quadrature part of the tensor ellipses (right-hand side of Fig. 14) at $T = 0.06$ s. This response is shown more clearly by the coordinate-invariant phase Φ_0 shown as contours. The small phase shift seen is a measure of the eddy currents induced into the upper part of the conductor, which is also reflected in the alignment of the quadrature tensor ellipse major axes at $T = 0.06$ s. At longer periods or when the source–receiver offset is comparable to the skin depth the phase rises towards 90° as can be seen in the lower right-hand corner of the $T = 0.06$ and 0.6 s quadrature tensor maps (Fig. 14).

DISCUSSION

Initial analysis of CSMT data using the impedance tensor ignores information concerning the source. It seems to us that it is a retrograde step to take two independent data sets (**E** and **H**), each of which will contain noise, in order to derive the impedance tensor in a situation where the source information is readily available. The apparent resistivity tensor is a simple way of including this information in the data analysis. Compared with the MT apparent resistivity based on the impedance tensor, the electric apparent resistivity tensor is well behaved over the entire frequency range used for CSMT surveys. Thus, using the electric field apparent resistivity tensor, the problems that arise from the ambiguity in the range of validity of the MT approximation can be avoided. A preliminary image of the (3-D) conductivity structure can also be constructed directly from the field data with little computational effort. This image will be independent of the coordinate system used to represent the data.

At longer periods the information concerning the subsurface is dominantly contained in the electric field. In situations where the target structure is 3-D, large numbers of measurement sites are needed to image the structure. The expense and complexity of the equipment needed to collect both electric and magnetic field data simultaneously and the insensitivity of the magnetic field to the conductivity structure suggest that a more *cost effective* exploration strategy for grounded source surveys might be to record only the electric field data at a large number of sites and to dispense with the measurements of the horizontal magnetic field. This approach would mirror the practice in industrial MT surveys where the magnetic field is recorded at only a small subset of sites, with the horizontal magnetic field measurements playing the role of the source field (**J**) in our representation.

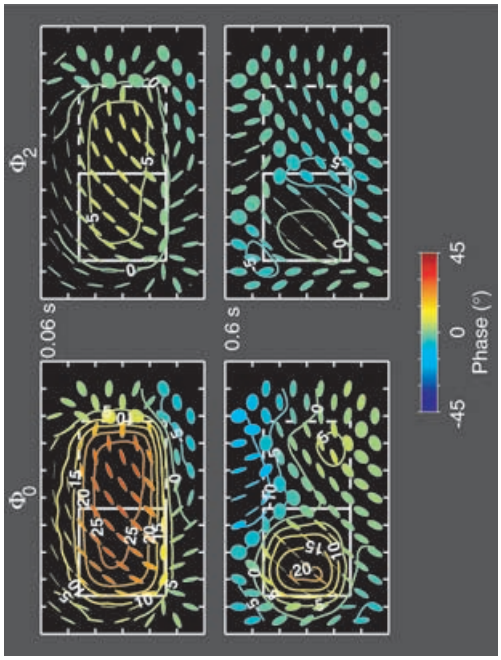

Figure 13. Quadrature electric field apparent resistivity tensor ellipse maps at two different periods for the model shown in Fig. 11. The ellipse colour and contour values indicate the coordinate-invariant phases Φ_0 and Φ_2 in the left- and right-hand set of maps, respectively. The apparent resistivity ellipses in this figure have all been normalized so that the major axes of the ellipses are all of unit length.

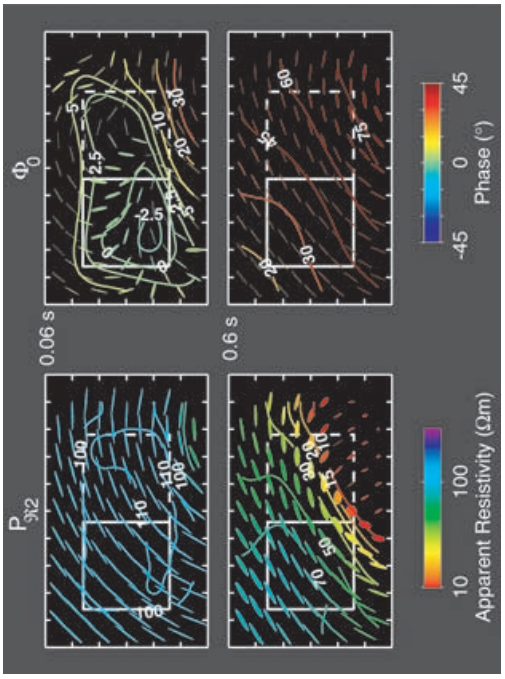

Figure 14. Magnetic field apparent resistivity tensor ellipse maps at two different periods for the model shown in Fig. 11. The ellipses in the left-hand set of maps show the in-phase part of the apparent resistivity tensor, the colour and contours indicating the value of the coordinate-invariant apparent resistivity $|P_{\Re 2}|$. The ellipses on the left have been scaled so that the lengths of the major axes are proportional to $\log(\rho_{\Re\,\max})$. The quadrature tensor ellipses are shown in the right-hand set of maps and have been scaled so that the major axes are of unit length. The ellipse colour and contour values in these maps indicate the determinant phase Φ_0.

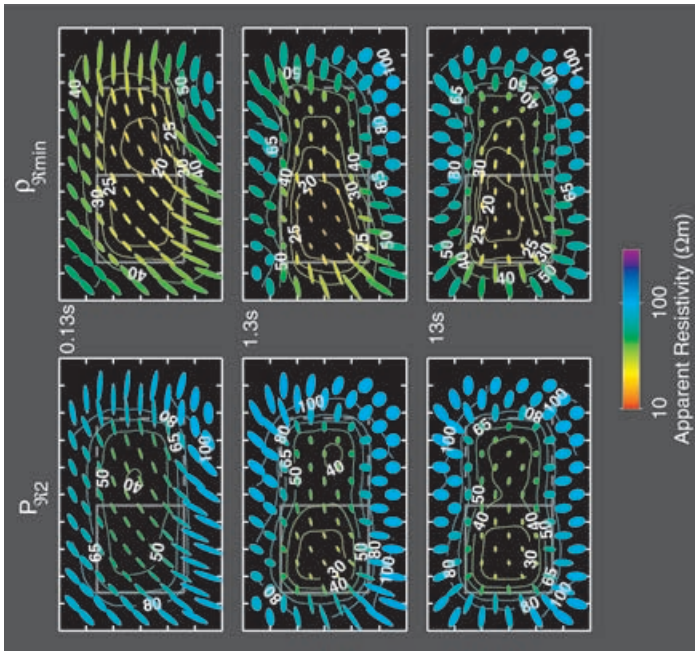

Figure 12. Frequency-domain in-phase electric field apparent resistivity tensor ellipses at three different periods for the 3-D model shown in Fig. 11. The colour of the ellipses and contours indicate the values of apparent resistivities $P_{\Re 2}$ and $\rho_{\Re\,\min}$ in the right and left-hand set of panels, respectively. The ellipses in this figure have been scaled so that the lengths of major axes are proportional to $\log(\rho_{\Re\,\max})$. The location of the sources is shown in Fig. 11.

The collection of early-time data in a TDEM survey is often difficult since it requires a wide bandwidth receiver and is 'open' to noise from a wide variety of sources. A frequency-domain approach to recording data in the equivalent time range would avoid this difficulty. Thus, a combination of time and frequency-domain recording techniques for grounded source surveys may prove to be easier in practice. The method of data analysis developed here provides a single mathematically consistent way of analysing the results of such surveys.

CONCLUSIONS

To fully characterize the electromagnetic field responses in a 3-D situation, the EM field must be recorded for at least two different polarizations. For the grounded source surveys this requires the use of two (or more) collocated source bipoles. We have shown that where two (or more) sources are used it is possible to analyse the horizontal magnetic and electric fields using a single mathematical representation in either the frequency or the time domain. In each case it is possible to derive a tensor apparent resistivity. To do this, information concerning the geometry and moment of the current sources must be incorporated into the analysis. A third vector field **J**, the DC current density in a uniform half-space appropriate to each source, is used to represent this information. Thus, in either the frequency or the time domain, three vector fields: the electric field **E**, the magnetic field **H** and **J**, represent the measurements. The relationship between any two of these fields is expressed by a tensor, the most familiar of which is the CSMT impedance tensor, which relates **E** and **H**. In previous work, Caldwell & Bibby (1998) demonstrated the utility of this approach for the analysis of time-domain electric fields, where **E** and **J** are related by an instantaneous apparent resistivity tensor $\boldsymbol{\rho}_a(t)$. In this paper we have introduced the less intuitive concept of an apparent resistivity tensor based on the horizontal magnetic field vector.

The tensor relationship between the source field **J** and the electric or horizontal magnetic fields provides a method of normalizing controlled source EM data that allows coordinate-invariant parameters to be derived directly from the observations. In this way, the horizontal components of the time or frequency-domain EM field produced by multiple-sources can be visualized in a compact and physically intuitive way. Our modelling results show that in simple 3-D situations the apparent resistivity images derived from the coordinate invariants of the *electric field* apparent resistivity tensor are remarkably good representations of the subsurface structure despite the simplicity of the imaging procedure. To a good approximation, these images will be independent of the current source orientation. Our results also demonstrate that the horizontal magnetic field components are largely insensitive to the localized 3-D conductivity structures that are usually the target of EM exploration surveys.

ACKNOWLEDGMENTS

Our thanks go to Zonghou Xiong and who made his 3-D modelling code available to us without which much of this work would not have been possible. Our work has also benefited from the many insightful discussions we have had with George Risk and Ian Reilly. Our thanks also go to Andreas Hördt and Ted Lilley for their careful reviews that helped clarify the paper. This work was supported by the Marsden Fund administered by the Royal Society of New Zealand (Institute of Geological and Nuclear Sciences contribution, 2263) and by the Enterprise Ireland Basic Research Grants Scheme (Project-SC-1998-501).

REFERENCES

Bibby, H.M., 1977. The apparent resistivity tensor, *Geophysics,* **42**, 1258–1261.

Bibby, H.M., 1986. Analysis of multiple-source bipole–dipole resistivity surveys using the apparent resistivity tensor, *Geophysics,* **51**, 972–983.

Bibby, H.M., 1994. Reply to comment on 'Three dimensional interpretation of multiple-source bipole–dipole resistivity data using the apparent resistivity tensor', by Xiaobo, L. & Pedersen, L.B., *Geophys. Prospect.,* **42**, 527–529.

Bibby, H.M. & Hohmann, G.W., 1993. Three dimensional interpretation of multiple-source bipole–dipole data using the apparent resistivity tensor, *Geophys. Prospect.,* **41**, 697–723.

Bibby, H.M., Dawson, G.B., Rayner, H.H., Stagpoole, V.M. & Graham, D.J., 1984. The structure of Mokai geothermal field based on geophysical observations, *J. Volc. Geotherm. Res.,* **20**, 1–20.

Caldwell, T.G. & Bibby, H.M., 1998. The instantaneous apparent resistivity tensor: a visualisation scheme for LOTEM electric field measurements, *Geophys. J. Int.,* **135**, 817–834.

Caldwell, T.G., Bennie, S.L., Keen, D.E. & Graham, D.G., 1999. Long-offset transient electromagnetic measurements at the Wairakei Geothermal field, *Proc. 21st NZ Geothermal Workshop 1999,* University of Auckland.

Chave, A.D. & Smith, J.T., 1994. On electric and magnetic galvanic distortion tensor decompositions, *J. geophys. Res.,* **99**, B3, 4669–4682.

Edwards, R.N. & Nabighan, M.N., 1991. The magnetometric resistivity method, in *Electromagnetic Theory for Geophysical Applications,* Vol. 2, ed. Nabigian, M.N., Applications, Society of Exploration Geophysicists, Tulsa.

Hördt, A., Jödicke, H., Strack, K.-M., Vozoff K. & Wolfgram, P.A., 1992. Interpretation of long-offset TEM soundings near the borehole at Munsterland 1, Germany, and comparison with MT measurements, *Geophys. J. Int.,* **108**, 930–940.

Jiracek, G.R., 1990. Near-surface and topographic distortions in electromagnetic induction, *Surv. Geophys.,* **11**, 163–203.

Kaufman, A.A. & Keller, G.V., 1983. *Frequency and Transient Soundings,* Elsevier, Amsterdam.

Keller, G.V. & Frischknecht, F.C., 1966. *Electrical Methods in Geophysical Prospecting,* Pergamon, Oxford.

Li, X. & Pedersen, L.B., 1991. Controlled source tensor magnetotellurics, *Geophysics,* **56**, 1456–1461.

Li, X. & Pedersen, L.B., 1994. Comment on 'Three dimensional interpretation of multiple-source bipole–dipole resistivity data using the apparent resistivity tensor, by Bibby H.M. & Hohmann, G.W., *Geophys. Prospect.,* **42**, 525–526.

Mase, G.E., 1970. *Continuum Mechanics,* McGraw-Hill, New York.

Newman, G.A., 1989. Deep transient sounding with a grounded source over near surface conductors, *Geophys. J. Int.,* **98**, 587–601.

Nye, J.F., 1957. *Physical Properties of Crystals,* Oxford University Press, London.

Pellerin, L., Johnston, J.M. & Hohmann, G.W., 1996. A numerical evaluation of electromagnetic methods in geothermal exploration, *Geophysics,* **61**, 121–130.

Qian, W. & Pedersen, L.B., 1992. Near surface distortion effects on controlled source tensor magnetotellurics, *Geophysics,* **58**, 1507–1510.

Raiche, A.P. & Gallagher, R.P., 1985. Apparent resistivity and diffusion velocity, *Geophysics,* **50**, 1628–1633.

Risk, G.F., Bibby, H.M. & Caldwell, T.G., 1993. DC resistivity mapping with the multiple-source, bipole–dipole array in the Central Volcanic Region, New Zealand, *J. Geomag. Geoelectr.,* **45**, 897–913.

Routh, P.S. & Oldenburg, D.W., 1999. Inversion of controlled source audio frequency magnetotellurics data for a horizontally layered earth, *Geophysics,* **64**, 1689–1697.

Spiegel, M.R., 1968. *Mathematical Handbook,* McGraw-Hill, New York.

Spies, B.R. & Eggers, D.E., 1986. The use and misuse of apparent resistivity in electromagnetic methods, *Geophysics,* **51**, 1462–1471.

Spies, B.R. & Frischknecht, F.C., 1991. Electromagnetic sounding in electromagnetic methods in applied geophysics, in *Electromagnetic Theory for Geophysical Applications,* Vol. 2, ed. Nabigian, M.N., Applications, Society of Exploration Geophysicists, Tulsa.

Strack, K.-M., 1992. *Exploration with Deep Transient Electromagnetics,* Elsevier, Amsterdam.

Szarka, L. & Menvielle, M., 1997. Analysis of rotational invariants of the magnetotelluric impedance tensor, *Geophys. J. Int.* **129**, 133–142.

Wait, J.R., 1961. The electromagnetic fields of a horizontal dipole in the presence of a conducting half-space, *Can. J. Phys,* **39**, 1017–1028.

Wannamaker, P.E., 1997. Tensor CSAMT survey over the Sulphur Springs thermal area, Valles Caldera, NM, Part II: Implications for CSAMT methodology, *Geophysics,* **62**, 466–476.

Ward, S.H. & Hohmann, G.W., 1988. Electromagnetic theory for geophysical applications, in *Electromagnetic Methods in Applied Geophysics,* Vol. 1, ed. Nabigian, M.N., Theory, Society of Exploration Geophysicists, Tulsa.

Weaver, J.T., Agarwal A.K. & Lilley, F.E.M., 2000. Characterisation of the magnetotelluric tensor in terms of its invariants, *Geophys. J. Int.,* **141**, 321–336.

Xiong, Z., 1992. Electromagnetic modelling of three-dimensional structures by the method of system iteration using integral equations, *Geophysics,* **57**, 1556–1561.

Xiong, Z. & Tripp, A., 1995. A block iterative algorithm for 3D electromagnetic modelling using integral equations with symmetrized substructures, *Geophysics,* **60**, 291–295.

Zohdy, A.A.R., 1978. Total field resistivity mapping and soundings over horizontally layered media, *Geophysics,* **43**, 748–766.

Zonge, K.L. & Hughes, L.J., 1991. Controlled source audiomagnetotellurics, in *Electromagnetic Methods in Applied Geophysics,* Vol. 2B, ed. Nabigian, M.N., Application, Society of Exploration Geophysicists, Tulsa.

APPENDIX A

To develop an apparent resistivity tensor ($\boldsymbol{\rho}_{\mathbf{H}}$) from the components of the magnetic field we must find a quadratic form of $\boldsymbol{\xi}$ that transforms as a second-rank tensor. By analogy with the electric field apparent resistivity, we also require the P_2 invariant of the magnetic field apparent resistivity tensor $\boldsymbol{\rho}_{\mathbf{H}}$ to have the same value as the resistivity of a uniform half-space where the source–receiver offset is much greater than the corresponding diffusion or skin depth. In particular, we will require the magnetic field apparent resistivity in this limit to have the same form as the resistivity tensor of a half-space made up of a *uniformly anisotropic* material with one of its principal axis in the vertical direction. That is, in a Cartesian coordinate system (x, y) aligned with the principal axes of the anisotropic half-space, $\boldsymbol{\rho}_{\mathbf{H}}$ must take the form

$$\boldsymbol{\rho} = \begin{bmatrix} \rho_{xx} & 0 \\ 0 & \rho_{yy} \end{bmatrix}. \tag{A1}$$

Although the resistivity tensor of a homogenous material is symmetric for thermodynamic reasons (e.g. Nye 1957) these conditions do not apply to the apparent resistivity tensor. In particular, $\boldsymbol{\rho}_{\mathbf{H}}$ must also be non-symmetric if it is to represent the asymmetries present in the magnetic field in the general case, i.e. when the conductivity distribution is 3-D.

The most general second-rank tensor quadratic form that can be formed from $\boldsymbol{\xi}$ is a linear combination of the contractions or inner products (second-rank tensors) of the tensor (or outer) product $\boldsymbol{\xi} \otimes \boldsymbol{\xi}$, which is a fourth-rank tensor (Mase 1970). In an orthogonal coordinate system the tensor product $\mathbf{Q} = \boldsymbol{\xi} \otimes \boldsymbol{\xi}$ can be written in terms of its components as

$$\mathbf{Q}_{ijkl} = \xi_{ij}\xi_{kl}, \tag{A2}$$

where the subscripts or indices in (for example) a Cartesian coordinate system denote the x and y coordinates. The inner product or contraction of a tensor is obtained by summing over a pair of indices, reducing the rank of the tensor by two. There are five independent contractions of $\mathbf{Q}$. In component form these can be written as $\mathbf{Q}(1,2) = \xi_{kk}\xi_{ij}$, $\mathbf{Q}(1,3) = \xi_{ki}\xi_{kj}$, $\mathbf{Q}(1,4) = \xi_{ki}\xi_{jk}$, $\mathbf{Q}(2,3) = \xi_{ik}\xi_{kj}$ and $\mathbf{Q}(3,4) = \xi_{ik}\xi_{jk}$; where the repeated subscript (k) represents a sum over the coordinate indices and the integer arguments denote the indices included in the summation. Equivalently, in matrix notation: $\mathbf{Q}(1,2) = \mathrm{tr}(\boldsymbol{\xi})\boldsymbol{\xi}$, $\mathbf{Q}(1,3) = \boldsymbol{\xi}^{\mathrm{t}}\boldsymbol{\xi}$, $\mathbf{Q}(1,4) = (\boldsymbol{\xi}\boldsymbol{\xi})^{\mathrm{t}}$, $\mathbf{Q}(2,3) = \boldsymbol{\xi}\boldsymbol{\xi}$ and $\mathbf{Q}(2,4) = \boldsymbol{\xi}\boldsymbol{\xi}^{\mathrm{t}}$; where $\boldsymbol{\xi}^{\mathrm{t}}$ and $\mathrm{tr}(\boldsymbol{\xi})$ are the transpose and trace of the tensor matrix, respectively.

Where $r/\delta_{\mathrm{TD}} \gg 1$ (or in the frequency domain $r/\hat{\delta} \gg 1$) the horizontal components of the EM field produced by a dipole source on a uniformly anisotropic half-space are (locally) orthogonal and the EM field can be considered to be linearly polarized over a small area. In a Cartesian coordinate system oriented so that the axes directions coincide locally with the principal axes of the anisotropic half-space, $\boldsymbol{\xi}$ will have the same zero trace form at early times as it does in a homogenous isotropic half-space (eq. 11). That is, the horizontal electric and magnetic fields at the surface of an anisotropic half-space in the 'far field' ($r/\delta_{\mathrm{TD}} \gg 1$ or $r/\hat{\delta} \gg 1$) case are orthogonal and

$$\boldsymbol{\xi}(t \to 0^{+}) = \begin{bmatrix} 0 & \xi_{xy} \\ \xi_{yx} & 0 \end{bmatrix}. \tag{A3}$$

In this case ξ_{yx} and ξ_{xy} depend separately upon the resistivities ρ_{xx} and ρ_{yy}, respectively. Thus $\boldsymbol{\rho}_{\mathbf{H}}$ must be proportional to the tensor

$$\begin{bmatrix} \xi_{yx}^2 & 0 \\ 0 & \xi_{xy}^2 \end{bmatrix} = \mathbf{Q}(1,3). \tag{A4}$$

Since $\mathrm{tr}(\boldsymbol{\xi}) = 0$ in a uniform half-space we can add $\mathbf{Q}(1,2)$ to eq. (A4) without changing the tensor form. Thus the most general form of $\boldsymbol{\rho}_{\mathbf{H}}$ is a linear combination of $\mathbf{Q}(1,2)$ and $\mathbf{Q}(1,3)$, i.e.

$$\boldsymbol{\rho}_{\mathbf{H}} = \kappa[a\,\mathrm{tr}(\boldsymbol{\xi})\boldsymbol{\xi} + \boldsymbol{\xi}^{\mathrm{t}}\boldsymbol{\xi}], \tag{A5}$$

where a is an unknown constant and κ is given by $-(\mu_0\pi/4t)$ and $-i\omega\mu_0$ in the time and frequency domains, respectively. Since $\boldsymbol{\xi}^{\mathrm{t}}\boldsymbol{\xi}$ is symmetric, $\boldsymbol{\rho}_{\mathbf{H}}$ will be non-symmetric in the general 3-D case only if $a \neq 0$. Rewriting $\boldsymbol{\rho}_{\mathbf{H}}$ as

$$\boldsymbol{\rho}_{\mathbf{H}} = \kappa[a\,\mathrm{tr}(\boldsymbol{\xi})\mathbf{I} + \boldsymbol{\xi}^{\mathrm{t}}]\boldsymbol{\xi}, \tag{A6}$$

where $\mathbf{I}$ is the identity matrix, we can see that the determinant (i.e. P_2^2) is given by

$$\det(\boldsymbol{\rho}_{\mathbf{H}}) = \kappa^2 \det[a\,\mathrm{tr}(\boldsymbol{\xi})\mathbf{I} + \boldsymbol{\xi}^{\mathrm{t}}]\det(\boldsymbol{\xi}). \tag{A7}$$

In the 3-D case where $\mathrm{tr}(\boldsymbol{\xi}) \neq 0$, the requirement that the P_2 invariant of $\boldsymbol{\rho}_{\mathbf{H}}$ is equal to $\rho_{\det\xi}$, i.e. P_2 is linearly proportional to $[\det(\boldsymbol{\xi})]^2$ (eqs 17 or 46) implies

$$\det[a\,\mathrm{tr}(\boldsymbol{\xi})\mathbf{I} + \boldsymbol{\xi}^{\mathrm{t}}] = \det(\boldsymbol{\xi}). \tag{A8}$$

This condition reduces to the equation

$$a(a+1)\,\mathrm{tr}(\boldsymbol{\xi}) = 0. \tag{A9}$$

Since we require $a \neq 0$ and $\mathrm{tr}(\boldsymbol{\xi}) \neq 0$ in the 3-D case, this condition is satisfied if $a = -1$ and

$$\boldsymbol{\rho}_{\mathbf{H}} = -\kappa[\mathrm{tr}(\boldsymbol{\xi})\boldsymbol{\xi} - \boldsymbol{\xi}^{\mathrm{t}}\boldsymbol{\xi}]. \tag{A10}$$